Title: Conformational dynamics and role of the acidic pocket in ASIC pH-dependent gating.

Authors: Vullo S, Bonifacio G, Roy S, Johner N, Bernèche S, Kellenberger S

Journal: Proceedings of the National Academy of Sciences of the United States of America

Year: 2017 Apr 4

Issue: 114

Volume: 14

Pages: 3768-3773

DOI: 10.1073/pnas.1620560114

This manuscript has been published in PNAS on March 20, 2017, doi: 10.1073/pnas.1620560114
Link to the website: http://www.pnas.org/content/114/14/3768.long

Classification: BIOLOGICAL SCIENCES, Physiology

Conformational dynamics and role of the acidic pocket in ASIC pH-dependent gating

Sabrina Vullo*[†], Gaetano Bonifacio*[†], Sophie Roy[†], Niklaus Johner[‡], Simon Bernèche[‡] and Stephan Kellenberger[†]

[†], Department of Pharmacology and Toxicology, University of Lausanne, Rue du Bugnon 27, 1011 Lausanne, Switzerland
[‡], SIB Swiss Institute of Bioinformatics, Klingelbergstrasse 50/70, 4056 Basel, Switzerland; Biozentrum, University of Basel, Klingelbergstrasse 50/70, 4056 Basel, Switzerland

*, these authors contributed equally

Short title: Role of acidic pocket in ASIC gating

Correspondence to:
Stephan Kellenberger
Département de Pharmacologie et de Toxicologie
Rue du Bugnon 27
Université de Lausanne
CH-1011 Lausanne
Switzerland
Stephan.Kellenberger@unil.ch
phone ++4121 692 5422
fax ++4121 692 5355

Keywords: Acid-sensing ion channel | conformational changes | voltage-clamp fluorometry | kinetic model

Abstract

Acid-sensing ion channels (ASICs) are proton-activated Na^+ channels expressed in the nervous system where they are involved in learning, fear behaviors, neurodegeneration and pain sensation. In this work, we study the role in pH sensing of two regions of the ectodomain enriched in acidic residues, the acidic pocket, which faces the outside of the protein and is the binding site of several animal toxins, and the palm, a central channel domain. Using voltage-clamp fluorometry we find that the acidic pocket undergoes conformational changes during both activation and desensitization. Concurrently, we find that while proton sensing in the acidic pocket is not required for channel function, it does contribute both to activation and desensitization. Furthermore, protonation-mimicking mutations of acidic residues in the palm induce a dramatic acceleration of desensitization followed by the appearance of a sustained current. In summary, this work describes the roles of potential pH sensors in two extracellular domains, and it proposes a model of acidification-induced conformational changes occurring in the acidic pocket of ASIC1a.

Significance

Many physiological processes are regulated by pH. The acid-sensing ion channels (ASICs) are neuronal pH sensors involved in learning, fear behavior, neurodegeneration after ischemic stroke, and pain sensation. The mechanism by which acidic pH activates ASICs is still poorly understood. We show here that the "acidic pocket", the binding site of several toxins, is not essential for channel function, but has rather a modulatory role. Furthermore, we describe the structural

rearrangements occurring in this domain during ASIC activity, and highlight the importance of the "palm" domain in channel opening and current decay. In this study we provide new insights on the molecular mechanisms controlling ASIC activity together with a rational basis for the development of ASIC-targeting drugs.

\body

Acid-sensing ion channels (ASICs) are Na^+-permeable channels (1) that participate in neuronal signaling under conditions involving pH changes, such as neuronal activity, ischemia and inflammation. ASICs are involved in fear behaviors, learning, neurodegeneration after ischemic stroke, and in pain sensation (2, 3). Functional ASICs are composed of three identical or homologous subunits (4, 5).

These channels respond to extracellular acidification with a transient current, because rapidly after opening they enter a non-conducting, so-called "desensitized" functional state. Crystal structures of chicken ASIC1 (~90 % sequence homology to human ASIC1a) reveal presumably desensitized (5, 6) and toxin-opened conformations (7-9). Single ASIC subunits have a shape similar to that of a hand holding a small ball (5), and thus their domains have been named accordingly (Fig. 1A). The palm domain forms the internal scaffold of the channel along the central vertical axis. The thumb and the finger point towards the exterior of the channel and enclose together with the β-ball the "acidic pocket" (AcP), a region containing many acidic residues (Fig. 1A, (5)).

Due to the presence of many acidic residues, the AcP was initially proposed as pH sensor of ASICs (5). Although mutation of AcP Glu and Asp residues shifts the pH dependence of ASIC activation to more acidic values (5, 10-12), H^+-sensing residues have also been identified outside the AcP (10, 12, 13), indicating that the AcP is not the only extracellular pH sensing domain. Its importance is however underlined by the fact that it constitutes the binding site of several ASIC-specific toxins (7, 14).

In the present study we asked whether acid sensing in the AcP and the palm is required for ASIC activation and whether the timing of conformational changes in the AcP is compatible with a role in activation. We show that combined, conservative mutation of potential pH-sensing residues in the AcP changes the pH dependences, but still allows ASIC opening and desensitization. Analogous mutations in the palm accelerated desensitization and led to the appearance of a secondary, sustained current. Voltage-clamp fluorometry (VCF) analysis indicates the occurrence of rapid and slow conformational changes in the AcP, compatible with a role in both activation and desensitization, and allows us to propose a model of conformational changes in this domain.

Results

Acidic residues in the acidic pocket are not required for ASIC activation. To determine the importance of pH sensing in the AcP for ASIC1a function we combined neutralization mutations of all Asp, Glu and His residues of the AcP to Asn or Gln (Fig. 1A-B). When all the protonable residues of the AcP were mutated, these channels, expressed in *Xenopus* oocytes, still produced transient currents upon extracellular acidification. Some mutants displayed up to two-fold accelerated kinetics of current decay (Fig. S1A) in accordance with previous studies that described altered current kinetics of AcP mutants (15, 16). Some mutants showed a sustained current, which was however small in all mutants except AcP16b (Fig. S1B), indicating that desensitization is in most mutants complete at the end of an acidification.

The pH inducing half-maximal activation (pH50) was generally shifted by ~0.5 pH units to more acidic values compared to WT (green symbols and bars in Fig. 1D-E).

The Hill coefficient, a measure of the steepness of the pH-current relationship and of the cooperativity of the process, decreased from ~3 in WT to ~1.5 in most channels containing more than seven AcP mutations (grey bars in Fig. 1E). The pH dependence of steady-state desensitization (SSD), the direct transition from the closed to the desensitized state (blue arrow in the scheme of Fig. 1D), was determined by exposing oocytes to a series of conditioning test pH solutions during 55 s, each followed by a short application of an acidic pH solution. The pH dependence of SSD was shifted to more alkaline values by the combination of AcP mutations (blue symbols and bars in Figs. 1D & F), although less so for constructs containing > 14 neutralization mutations.

As shown above, neutralization mutations of protonable residues in the AcP induced the following functional changes: 1) they shift the pH50 of activation to more acidic values; 2) they shift the pH50 of SSD to more alkaline values, and 3) they decrease the Hill coefficient of activation, but not of SSD. Neutralization mutations of Asp and Glu, mimicking protonated acidic residues, correspond to gain of function mutations, which are expected to lead to an alkaline shift in pH dependence as observed for neutralization mutations of key proton-sensing residues in the K^+ channel KcsA (17). Although our mutagenesis approach does not indicate whether a mutated residue is a pH sensor or has other roles in conformational transitions, it is very likely that at least some of these residues are pH sensors. Since the observed effects of AcP mutations appear to be complex, we use kinetic models to illustrate how these mutations may affect pH dependence. Consider a 4-state model as depicted in Fig S1C, corresponding to a system with 2 protonation sites, either of which can be protonated or not. A neutralization mutation will correspond to having one of the sites always protonated, reducing the problem to a 2-state model. We

show that if protonation of both sites is required for the transition to the state of interest (e.g the open state), then a neutralization mutation will always lead to an increase in pH50 accompanied by a decrease of the Hill coefficient (*SI Methods* and Fig. S1D). But if protonation of only one of the sites is required, then mutation of the other one can lead to both an increase or a decrease in pH50, as well as an increase or a decrease in the Hill coefficient (Fig. S1D and S1E, *SI Methods*). The observed effects of AcP mutations therefore suggest a non-essential role of this domain in activation. To test this hypothesis, we have built a kinetic model of ASIC comprising three sets of protonation sites: 1) sites in the AcP, 2) other sites responsible for desensitization, and 3) sites leading to activation (Fig. S1F and *SI Methods*). The model was fitted to traces of complete activation and SSD curves of ASIC1a WT and the mutants AcP11 and AcP14. The model reproduced the experimental data reasonably well if protonation of the AcP was considered accessory for activation, regardless of whether the same protonation events in the AcP were modeled as required or accessory for desensitization (Figs. 1G-H and S1F), but not if they were considered essential for activation. The parameters of the fitted models indicated that protonation of the AcP shows a negative cooperativity with protonation of activation sites, and a positive cooperativity with protonation of desensitization sites. The modeling suggests therefore that protonation-mimicking mutations of the AcP induced an acidic shift in activation pH dependence due to the negative cooperativity between these two types of protonation.

Combined mutations of potential pH sensors in the palm accelerate desensitization and give rise to a non-desensitizing current. To assess the role of pH sensing in the palm, we combined mutations of the six acidic residues of the

lower and middle palm (palm core, "PaC", bold in Fig 2A), and subsequently in addition the two nearby β-ball residues D212 and E254 (Fig. 2A-B). The most striking feature of these combined mutants is the appearance of a sustained current component and with increasing number of mutations a complete disappearance of the transient current (Figs. 2C and S2A). The disappearance of the peak current could be either due to loss of channel activation or very fast desensitization. To test this, we measured the mutant channels at a lower temperature, which is known to strongly slow down desensitization but not activation (18). We uncovered a peak current in PaC6, and observed a strong increase of the PaC4 peak current amplitude relative to that of the sustained current (Figs. 2D and S2B). This demonstrates that the combined mutations such as PaC6 accelerate desensitization to an extent that the transient current disappears.

The slowly developing sustained current is only induced by cumulative palm mutations, as no single neutralization mutation of acidic residues of the palm did, except for D78, induce any sustained currents (Fig. S2C). This sustained current is distinct from the transient current with regard to several properties. 1) In contrast to the wt peak current it has almost completely lost its cation selectivity (Fig. S2D-G; P_{Na}/P_K ratio of 9.8 ± 0.4, 5.2 ± 0.4, 2.5 ± 0.3 and 2.7 ± 0.9 for wt, PaC4 peak, PaC4, and PaC6 sustained current, respectively, n=3-11, $p<0.01$); 2) it is not inhibited by the pore blocker amiloride (Fig. S2H-I); and 3) its pH dependence of activation is shifted by two pH units to more acidic values (Fig. 2E).

Additional mutation of the two acidic palm residues pointing towards the wrist, D78 and E421, or the wrist residue H73 (Fig. S2J) in PaC mutants did not further change the current properties in most cases (Fig. S2K-N). In two of these mutants a transient current was reconstituted. The pH dependence of the tested palm mutants correlated

with the type of current – transient vs sustained – and not with the number of mutations (Figs. 2E and S3M). This correlation together with the different current properties further confirm that these non-desensitizing currents are profoundly different types of openings, and may be related to sustained ASIC currents induced by some chemical compounds and lipids (19, 20).

Conformational changes in the acidic pocket. By which mechanisms do the palm and the AcP influence ASIC function? The comparison of toxin-opened and desensitized ASIC structures showed evidence for a centripetal movement of the three lower palm domains during desensitization (7). Accessibility studies combined with molecular dynamics simulations suggested that this conformational change in the palm is transduced into closure of the pore (21).

To obtain information on possible conformational changes in the AcP during gating, we applied VCF, which employs simultaneous measurement of ionic currents and of the fluorescence intensity of fluorophores placed at specific sites of the channel (Fig. 3A). Attachment of the fluorophores AlexaFluor488 (Fig. 3B) or CF488A to engineered Cys residues at different positions of the AcP did in most mutants not lead to measurable fluorescence changes (ΔF) during channel activity (Table S1). Changes in fluorescence intensity of fluorophores are due to alterations in the environment and/or quenching by nearby amino acid residues. Trp is known as a strong fluorescence quencher (22). To allow the measurement of ΔF signals in this domain, we have paired engineered Cys residues as fluorophore docking positions with engineered Trp residues as quenchers across the AcP (Figs. 3A and S3A).

Cys/Trp double mutants of the AcP produced transient acid-induced currents, and various types of ΔF signals. The ΔF of several Cys/Trp mutants contained two

components, an initial rapid negative or positive ΔF that was followed by a slower ΔF of the opposite polarity, as illustrated by current and ΔF traces of the mutant D347C/T236W (Fig. 3C, lower trace). To associate ΔF signals with functional transitions, we compared the kinetics of the ΔF and the current signals, measured as rise time (the time to pass from 10 to 90% of the full amplitude). We measured the pH 6-induced ΔF and currents from approximately the same oocyte surface by using a recording chamber in which the solution flows under the oocyte (Fig 3D; *SI Methods*). The onset kinetics of the fast ΔF component of the mutants D347C/T236W, D237C/D347W, D351C/D237W and E355C match the kinetics of current appearance (Figs. 3E and S3B; see Table S2 for a correlation analysis). These ΔF signals started 100-250 ms before the current (Fig. 3F-G), strongly suggesting that the monitored movements in these mutants are correlated with channel opening. The second ΔF components and the ΔF signals of all other mutants were slower than current appearance (Fig. 3E) and the difference in delay was smaller or absent. The ΔF onset was in most mutants faster than the current decay (Fig. 3H), and only two mutants, K343C/T236W and D351C/F257W, showed ΔF onset kinetics correlated with current desensitization. The transitions occurring after channel opening may thus be associated with desensitization or with its preparation.

The pH dependence of the ΔF signals was in most mutants close to that of SSD, and more alkaline than the pH dependence of current activation (Fig. 3I), hence these conformational changes could be part of channel desensitization. The ΔF signals sharing the kinetics of current appearance also showed such a shifted pH dependence, indicating that they occur at more alkaline pH than channel opening. This does not rule out their possible implication in channel opening, but indicates that there must be other conformational changes required for activation, which have

a lower pH50 than those occurring in the acidic pocket and would therefore govern the pH50 of activation. This shift in pH dependence is reminiscent of the leftward shift in voltage dependence of ΔF versus currents in voltage-gated K^+ channels (23, 24).

Hypothesized movements based on VCF observations. The proximity of a quenching group decreases the total fluorescence (F) of a fluorophore, but may generate an activity-induced fluorescence change (ΔF) if there is a change in distance between the fluorophore and the quenching group. The specific ΔF signals of the single Cys mutants used in the Cys/Trp pairs were of very small amplitude compared to the ΔF signal of related Cys/Trp pairs (Table S1), indicating that the ΔF observed in double mutants is due to the additional presence of the engineered Trp. Control experiments showed that the only endogenous Trp residue in the proximity of the palm, W233, did not affect these signals (compare Figs. S3C and 4A). A positive ΔF indicates therefore an increase in distance between the Trp residue and the Cys-attached fluorophore, whereas a negative ΔF indicates a decrease in this distance. These ΔF signals do not exactly reflect the distance changes between the Cys and Trp of a given pair, since the fluorophore has itself a diameter of 7-10 Å and is attached to the Cys residue by a linker (Fig. 3B), with an estimated distance between the docking site and the center of the fluorophore of 5-15 Å (from MD trajectories, Corry research group, http://karri.anu.edu.au/handy/). This limitation has to be considered as a factor of imprecision in the following interpretation of the VCF data.

The nature of the ΔF signals of different Cys/Trp double mutants (Fig. 4A) is summarized in the ASIC structure (Fig. 4B) with dotted lines between the paired residues and with "+" indicating an increase, and "-" a decrease in ΔF. The early,

rapid ΔF signals suggest therefore a short-lived approach of D237 towards D347 and D351, and an increase of the T236-D347distance, which occurs during or slightly before activation. The VCF analysis suggests that these movements are then followed by a decrease of the N120–K343 and T236–D347 distance, and by an increase of the D237–D347, D237–D351 and E238–D347 distance, and – with the time course of desensitization, an increase of the F257–D351 and a decrease of the K343-T236 distance.

We estimate that the higher amplitude of the slower ΔF components is due to a larger conformational change, since in the ΔF signals composed of a rapid and slow component, the ΔF of both components depends on the quenching by the engineered Trp, and rapid and slow signals were compared within the same Cys/Trp pair. Most likely the conformational changes generating these ΔF signals are part of a continuous movement of the involved AcP domains. The initial, fast ΔF signals that are correlated with channel activation may represent a tilting of the finger loop that would bring D237 and E238, located at the lower end of the loop, closer to the α5 helix, and T236, which is higher up, away from the α5 helix (green arrows in Fig. 4C). The distance changes involving residues T236, D237 and E238 occurring after activation are best explained by a movement of this finger loop towards the outside of the protein (right orange arrow in Fig. 4C). This movement may involve a partial rotation of the loop, bringing thereby T236 closer to K343 and D347, as well as moving D237 and E238 away from D347 and D351. The α5 helix likely undergoes a movement relative to the other domains that brings its outer end (K343) closer to the finger and its inner part (D351) away from the β-ball.

ΔF signals in mutants containing protonation-impaired domains. To determine whether conformational changes depend on protonation events in the AcP and the palm, we introduced a fluorophore/quencher pair in the AcP mutant AcP13, and the E355C mutation in the palm mutant PaC5, thus two mutants in which a large number of acidic residues have been neutralized. In both, AcP13/N237C/N347W and PaC5/E355C the slow, but not the fast ΔF component was present (Figs. 4D and S4). The absence of a fast ΔF component in these mutants may be due to a requirement of protonation of AcP or palm residues for the rapid ΔF signal. We can however not exclude the possibility that this absence is due to a changed environment, especially for AcP13/N237C/N347W. The fact that the slower ΔF signal is still present in the combined mutants indicates that protonation of neither AcP nor palm residues is required for the slower conformational changes occurring in the AcP. E355C showed, as expected, faster current decay kinetics in the PaC5 background, and this acceleration was also reflected in the ΔF onset kinetics ($p<0.0001$ and <0.05, respectively, Fig. S4D).

Discussion

We show in this study that the presence of protonable residues in the AcP and the palm is not essential for ASIC activation but plays other roles: in the AcP, acidic residues allow the fine-tuning of ASIC pH dependence, whereas in the palm they control the desensitization kinetics and prevent the appearance of a sustained current. Our VCF analysis provides evidence of conformational changes in the AcP correlated to activation and desensitization, and proposes a likely sequence of conformational changes in the AcP upon extracellular acidification.

The observed acceleration of the desensitization kinetics in palm mutants was much stronger than kinetic changes of palm mutants investigated in previous studies (10, 21) and led to the disappearance of the transient current at room temperature. The fact that it was induced by mutations that mimic protonated side chains suggests that protonation events in the palm lead to desensitization.

The AcP is the binding site of the two gating modifier toxins PcTx1 and Mambalgin (7, 9, 25-27). Non-conservative mutations in the AcP of ASICs have induced strong changes in the pH dependence (11, 28), while conservative mutations of Asp and Glu residues induced modest (5, 12) or no changes in activation pH dependence (10). The acidic residues of the thumb α5 helix E344, D347, D351 and E355 that are at the center of the interaction with the finger loop, are better conserved between ASIC1a and ASIC2 (3 of 4) than between ASIC1a and ASIC3 (1 of 4), whose pH dependence is close to that of ASIC1a. These differences appear not to affect the conformational changes in the AcP, since at least the slow ΔF signals were still present after neutralization of many AcP residues (Fig. 4D). For ASIC2 it was shown that regions outside the AcP, mostly the first ~90 residues after the TM1 are critical for channel function (29, 30). These observations are consistent with an important regulatory, but not essential role of the AcP in ASIC activation. The AcP also controls the kinetics and pH dependence of desensitization (15, 16, 27), a role that is underlined here by the slow ΔF signals, which may reflect conformational changes leading to desensitization. In ENaC, the AcP may also have a regulatory role, since it was shown to contain a binding site for Na^+ involved in channel inhibition (31).

Experimental evidence for conformational changes in the AcP was recently provided by LRET measurements showing that the distance between residues of the thumb and the finger is decreased in the desensitized compared to the closed state (28). We

describe here the time course of this closing movement and suggest that it concerns rather the external end of the AcP, which opens on its inner side. Such a movement of the inner part of the AcP is supported by the recent observation that formation of a disulfide bond between the thumb residue E355C and R175C of the palm locks the channel in the closed state (32). The slower conformational changes in the AcP do not depend on protonation events in the AcP or the palm, indicating that these conformational changes in the AcP are induced by protonation events occurring outside the AcP or the palm. Protonation of AcP residues, or binding of ligands to the AcP may influence the kinetics and possibly the amplitude of these conformational changes and thereby modulate ASIC function.

Our observation of large ΔF signals occurring between opening and desensitization, suggesting conformational changes in the AcP, contradicts the findings with crystal structures of ASIC1, which show an almost identical conformation of the AcP in toxin-opened and desensitized channels (7). It is possible that the toxin-opened ASIC conformation studied in crystal structures is different from the H^+-opened conformation. Evidence for important conformational changes during ASIC desensitization comes from the observation that ASIC currents show a strong temperature dependence of desensitization. In contrast, the temperature dependence of activation is much weaker (18). This is consistent with the small amplitude ΔF signals correlated to activation and the large amplitude ΔF signals correlated to later events. The above-mentioned LRET experiments (28) and a recent Cys accessibility study (15) also suggest conformational changes in the AcP upon acidification. To affect channel activity, conformational changes in the AcP need to change the conformation of the ASIC pore. The downward movement of the internal end of the α5 helix during desensitization would likely be transmitted to the pore via the β-turn

structure that is part of a palm-thumb loop and interacts with the external end of the transmembrane domain, or via the palm.

Materials and Methods

WT and mutant human ASIC1a was expressed in *Xenopus laevis* oocytes. All experiments with *Xenopus* were carried out in accordance with the Swiss federal law on animal welfare. ASIC currents were measured by two-electrode voltage-clamp, and VCF experiments were carried out as described (33), with the exception that a different measuring chamber, allowing measurement of current and fluorescence from approximately the same oocyte surface, was used for the kinetics experiments. Kinetic models were fitted directly to the measured currents using the Data2Dynamics software (34). Data are presented as mean ± SEM. Individual experimental data points are provided in S.I. Detailed material and methods are provided in *SI Methods*.

Acknowledgements. We thank Cláudia Igutti Suenaga Lelli for having carried out some of the experiments, and Omar Alijevic, Olivier Poirot, Laurent Schild, Olivier Staub and Miguel van Bemmelen for their comments on the manuscript, Gustav Akk for the prototype of the recording chamber and Ruud Hovius for help with the construction of the recording chamber and for many discussions. This work was supported by Swiss National Science Foundation grant 31003A_153419 to S.K and by . the Swiss Foundation for Excellence and Talent in Biomedical Research and the FP 7 European Union Human Brain Project (grant No 604102) to S.B. Calculations were performed at the sciCORE (http://scicore.unibas.ch/) scientific computing core facility at University of Basel.

References

1. Yang L & Palmer LG (2014) Ion conduction and selectivity in acid-sensing ion channel 1. *J Gen Physiol* 144(3):245-255.
2. Wemmie JA, Taugher RJ, & Kreple CJ (2013) Acid-sensing ion channels in pain and disease. *Nature Rev. Neurosci* 14(7):461-471.
3. Kellenberger S & Schild L (2015) International Union of Basic and Clinical Pharmacology. XCI. Structure, Function, and Pharmacology of Acid-Sensing Ion Channels and the Epithelial Na^+ Channel. *Pharmacol Rev* 67(1):1-35.
4. Bartoi T, Augustinowski K, Polleichtner G, Grunder S, & Ulbrich MH (2014) Acid-sensing ion channel (ASIC) 1a/2a heteromers have a flexible 2:1/1:2 stoichiometry. *Proc Natl Acad Sci U S A* 111(22):8281-8286.
5. Jasti J, Furukawa H, Gonzales EB, & Gouaux E (2007) Structure of acid-sensing ion channel 1 at 1.9 A resolution and low pH. *Nature* 449(7160):316-323.
6. Gonzales EB, Kawate T, & Gouaux E (2009) Pore architecture and ion sites in acid-sensing ion channels and P2X receptors. *Nature* 460(7255):599-604.
7. Baconguis I & Gouaux E (2012) Structural plasticity and dynamic selectivity of acid-sensing ion channel-spider toxin complexes. *Nature* 489(7416):400-405.
8. Baconguis I, Bohlen CJ, Goehring A, Julius D, & Gouaux E (2014) X-ray structure of Acid-sensing ion channel 1-snake toxin complex reveals open state of a Na^+-selective channel. *Cell* 156(4):717-729.

9. Dawson RJ*, et al.* (2012) Structure of the Acid-sensing ion channel 1 in complex with the gating modifier Psalmotoxin 1. *Nature communications* 3:936.

10. Krauson AJ, Rued AC, & Carattino MD (2013) Independent contribution of extracellular proton binding sites to ASIC1a activation. *J Biol Chem* 288(48):34375-34383.

11. Li T, Yang Y, & Canessa CM (2009) Interaction of the aromatics Tyr-72/Trp-288 in the interface of the extracellular and transmembrane domains is essential for proton gating of acid-sensing ion channels. *J. Biol. Chem.* 284(7):4689-4694.

12. Liechti LA*, et al.* (2010) A combined computational and functional approach identifies new residues involved in pH-dependent gating of ASIC1a. *J Biol Chem* 285(21):16315-16329.

13. Paukert M, Chen X, Polleichtner G, Schindelin H, & Grunder S (2008) Candidate amino acids involved in H^+ gating of acid-sensing ion channel 1a. *J. Biol. Chem.* 283(1):572-581.

14. Mourier G*, et al.* (2016) Mambalgin-1 Pain-relieving Peptide, Stepwise Solid-phase Synthesis, Crystal Structure, and Functional Domain for Acid-sensing Ion Channel 1a Inhibition. *J Biol Chem* 291(6):2616-2629.

15. Krauson AJ & Carattino MD (2016) The Thumb Domain Mediates Acid-sensing Ion Channel Desensitization. *J Biol Chem* 291(21):11407-11419.

16. Kusama N, Harding AM, & Benson CJ (2010) Extracellular chloride modulates the desensitization kinetics of acid-sensing ion channel 1a (ASIC1a). *J Biol Chem* 285(23):17425-17431.

17. Posson DJ, Thompson AN, McCoy JG, & Nimigean CM (2013) Molecular interactions involved in proton-dependent gating in KcsA potassium channels. *J Gen Physiol* 142(6):613-624.

18. Askwith CC, Benson CJ, Welsh MJ, & Snyder PM (2001) DEG/ENaC ion channels involved in sensory transduction are modulated by cold temperature. *Proc. Natl. Acad. Sci. U. S. A.* 98(11):6459-6463.

19. Marra S*, et al.* (2016) Non-acidic activation of pain-related Acid-Sensing Ion Channel 3 by lipids. *EMBO J* 35(4):414-428.

20. Yu Y*, et al.* (2010) A nonproton ligand sensor in the acid-sensing ion channel. *Neuron* 68(1):61-72.

21. Roy S*, et al.* (2013) Molecular determinants of desensitization in an ENaC/degenerin channel. *FASEB J* 27(12):5034-5045.

22. Pantazis A & Olcese R (2012) Relative transmembrane segment rearrangements during BK channel activation resolved by structurally assigned fluorophore-quencher pairing. *J. Gen. Physiol.* 140(2):207-218.

23. Mannuzzu LM, Moronne MM, & Isacoff EY (1996) Direct physical measure of conformational rearrangement underlying potassium channel gating. *Science* 271(5246):213-216.

24. Cha A & Bezanilla F (1997) Characterizing voltage-dependent conformational changes in the shaker K^+ channel with fluorescence. *Neuron* 19(5):1127-1140.

25. Schroeder CI*, et al.* (2014) Chemical synthesis, 3D structure, and ASIC binding site of the toxin mambalgin-2. *Angew Chem Int Ed Engl* 53(4):1017-1020.

26. Salinas M*, et al.* (2014) Binding site and inhibitory mechanism of the mambalgin-2 pain-relieving peptide on acid-sensing ion channel 1a. *J Biol Chem* 289(19):13363-13373.

27. Chen X, Kalbacher H, & Grunder S (2005) The Tarantula Toxin Psalmotoxin 1 Inhibits Acid-sensing Ion Channel (ASIC) 1a by Increasing Its Apparent H^+ Affinity. *J. Gen. Physiol.* 126(1):71-79.

28. Ramaswamy SS, MacLean DM, Gorfe AA, & Jayaraman V (2013) Proton-mediated Conformational Changes in an Acid-sensing Ion Channel. *J Biol Chem* 288(50):35896-35903.

29. Schuhmacher LN, Srivats S, & Smith ES (2015) Structural domains underlying the activation of acid-sensing ion channel 2a. *Mol Pharmacol* 87(4):561-571.

30. Smith ES, Zhang X, Cadiou H, & McNaughton PA (2007) Proton binding sites involved in the activation of acid-sensing ion channel ASIC2a. *Neurosci Lett* 426(1):12-17.

31. Kashlan OB, Blobner BM, Zuzek Z, Tolino M, & Kleyman TR (2015) Na^+ Inhibits the Epithelial Na^+ Channel by Binding to a Site in an Extracellular Acidic Cleft. *J Biol Chem* 290(1):568-576.

32. Gwiazda K, Bonifacio G, Vullo S, & Kellenberger S (2015) Extracellular Subunit Interactions Control Transitions between Functional States of Acid-sensing Ion Channel 1a. *J Biol Chem* 290(29):17956-17966.

33. Bonifacio G, Lelli CI, & Kellenberger S (2014) Protonation controls ASIC1a activity via coordinated movements in multiple domains. *J Gen Physiol* 143(1):105-118.

34. Raue A*, et al.* (2015) Data2Dynamics: a modeling environment tailored to parameter estimation in dynamical systems. *Bioinformatics* 31(21):3558-3560.

35. Li P*, et al.* (2010) Site-specific fluorescence reveals distinct structural changes induced in the human rho 1 GABA receptor by inhibitory neurosteroids. *Mol Pharmacol* 77(4):539-546.

36. Hille B (2001) *Ion channels of excitable membranes* (Sinauer Associates, Sunderland) 3rd Ed.

37. Pettersen EF*, et al.* (2004) UCSF Chimera--a visualization system for exploratory research and analysis. *J. Comput. Chem.* 25(13):1605-1612.

38. Mukhtasimova N, Lee WY, Wang HL, & Sine SM (2009) Detection and trapping of intermediate states priming nicotinic receptor channel opening. *Nature* 459(7245):451-454.

39. Krashia P, Lape R, Lodesani F, Colquhoun D, & Sivilotti LG (2011) The long activations of alpha2 glycine channels can be described by a mechanism with reaction intermediates ("flip"). *J Gen Physiol* 137(2):197-216.

40. Raue A*, et al.* (2013) Lessons learned from quantitative dynamical modeling in systems biology. *PloS one* 8(9):e74335.

Figure legends

Fig. 1. Combined mutation of acidic pocket residues preserves almost normal ASIC1a function. *(A)* Structural image, showing a human ASIC1a model based on the chicken ASIC1 structure (8). Left, trimer structure, individual domains of one subunit are colored and labeled. Right, close-up view of the AcP formed by the thumb, the finger and the β-ball. The residues that were mutated are indicated. *(B)*

Mutant composition. Each number in the right column represents a neutralization mutation, Glu to Gln, Asp to Asn, His to Asn. The new mutations from one construct to another are marked in red. *(C)* Representative current traces of WT and the mutant AcP11. The pH protocol is schematically indicated on the left. *(D)* pH dependence of activation and steady-state desensitization (SSD) of WT and AcP11 (n=4-6). Normalized current amplitudes are plotted as a function of stimulation pH for activation (filled symbols) and as a function of the conditioning pH for SSD (open symbols). The solid lines represent fits to the Hill equation (*SI Methods*). The kinetic scheme of ASIC functional states is shown, emphasizing with a green arrow the activation, and with a blue arrow the SSD transition. *(E)* pH dependence of activation, plotting pH of half-maximal activation (pH50) values, as green bars (left axis), and the Hill coefficient (nH) in grey (right axis). The conditioning pH in these experiments was 7.6-8.0, depending on the mutant, to ensure stable recordings without occurrence of SSD. For each mutant, the numbers in red indicate the residues mutated in addition to the mutations already present in the preceding mutant; n=4-125. *(F)* pH dependence of SSD, showing pH of half-maximal SSD, pHDes50 values as blue bars, and nH values of SSD in grey; n=5-56. *(G)* Experimental current traces (black) of an activation curve of ASIC1a WT and corresponding traces generated by the 32-state model (*SI Methods*). *(H)* Activation and SSD curves of WT, AcP11 and AcP14 generated experimentally (filled symbols) or by the 32-state model (open symbols). *, $p<0.05$, **, $p<0.01$, ***, $p<0.001$ and ****, $p<0.0001$, different from WT.

Fig. 2. Combined mutations of palm residues accelerate desensitization and induce a sustained current. *(A)* Structural image of the palm (yellow) and β-ball

(orange) domains of one ASIC1a subunit, showing the acidic residues investigated here, with residues of the "palm core" (see text) highlighted in bold. *(B)* Mutant composition. "PaC" stands for "palm core", "B" for "β ball". The new mutations from one construct to another (compared to the construct with lower number of mutations) are marked in red. *(C)* Representative current traces of different palm mutants. The vertical bar corresponds to (in μA): 6 (WT), 3 (PaC3), 4 (Pa4b), 1 (PaC4), 1.25 (PaC5), 0.5 (PaC6), 0.24 (PaC6.2B). *(D)* Representative current recordings of WT, PaC4 and PaC6 at the indicated temperatures. The vertical bar corresponds to (in μA): 4.6 (WT), 3.2 (PaC4), 1 (PaC6). (*C, D*) The conditioning pH was 7.4. *(E)* pH dependence of activation, pH50 values (colored bars) and nH of activation (grey bars), n=5-128. pH50 values of transient currents are shown in purple, of sustained currents in orange. *, $p<0.05$, **, $p<0.01$, ***, $p<0.001$ and ****, $p<0.0001$, different from WT.

Fig. 3. Fluorescence changes in the acidic pocket associated with channel opening and desensitization. *(A)* close-up view of the AcP, showing the residues that were mutated to Cys (to dock fluorophores) and/or to the quenching residue Trp. *(B)* Structure of the fluorophore AlexaFluor488. *(C)* representative current and ΔF traces at pH 7 and 6 of the mutant D237C/D347W, highlighting in green and blue the parts of the pH 6 traces used for kinetic analysis. Note that the ΔF trace has two components, as highlighted with the arrows. *(D)* Schematic view of the oocyte recording chamber used for measurements of current and ΔF kinetics (*SI Methods*). *(E)* Scatter graph comparing the rise time of the channel opening (black) and the ΔF onset (red) in response to acidification from the conditioning pH 7.4 to the stimulation pH 6 in paired experiments, n=6-12. For mutants containing two ΔF

components, the two are distinguished as 1st and 2nd. Correlation between the ΔF and current signal is indicated by labeling in bold turquoise (see criteria in Table S2). *(F)* Representative current and ΔF traces showing a mutant in which the start of the ΔF signal precedes that of the current (D347C/T236W, left) and one in which the two signals start at the same time (D347C/E238W, right). The vertical dashed line indicates the beginning of the ΔF. *(G)* Scatter dot plot of the difference in the ΔF and current delay of appearance ($delay_{\Delta F}$-$delay_I$) measured at pH 6, n=5-11. *(H)* Scatter graph comparing the current decay time (black) and the fluorescence rise time (red) in response to acidification from pH 7.4 to pH 6 in paired experiments, n=6-12. Bold turquoise labels indicate correlation between ΔF onset and current decay kinetics (Table S2). The inset shows in blue the parts of current and ΔF traces whose kinetics were compared. *(I)* pH of half-maximal amplitude (pH50) for current (black columns) and fluorescence activation (red), and of current SSD (green), n=4-16.

Fig. 4. Predicted conformational changes in the acidic pocket. *(A)* representative, paired current (black) and fluorescence (red) traces of double mutants in response to extracellular acidification to pH6. Black arrows point to fast ΔF components. *(B)* View of the AcP with the mutated residues, indicating by dashed black lines the different Cys/Trp pairs. For each double mutant the nature of the ΔF signal is indicated by "+" or "-" signs ("+" = increase in ΔF); for mutants with composite ΔF signal, the left sign represents the first component. *(C)* Scheme indicating the deduced conformational changes in the AcP during opening and steps preceding and correlated with desensitization, as discussed in the text. The grey cylinders represent residues mutated for the VCF experiments. The dotted outlines of the finger loop and

α5 thumb helix represent their hypothesized position in the closed state. Hypothesized conformational changes are illustrated by arrows, the green arrows standing for conformational changes occurring during activation, the orange for subsequent steps occurring before and during desensitization. *(D)* Representative current and ΔF traces of the mutants AcP13/N237C/N347C, AcP13/N237C and PaC5/E355C. Note that not only the N237C/N347W pair, but also the single mutation N237C induced measurable ΔF signals, indicating that in the changed environment of the AcP13 mutant, the N237C ΔF did not depend on the presence of a nearby Trp residue and does not reflect a change in distance between the fluorophore and the Trp residue. The PaC5/E355C mutant showed in ~ half of the experiments a rapid transient and a sustained component, and in the other half only a sustained current.

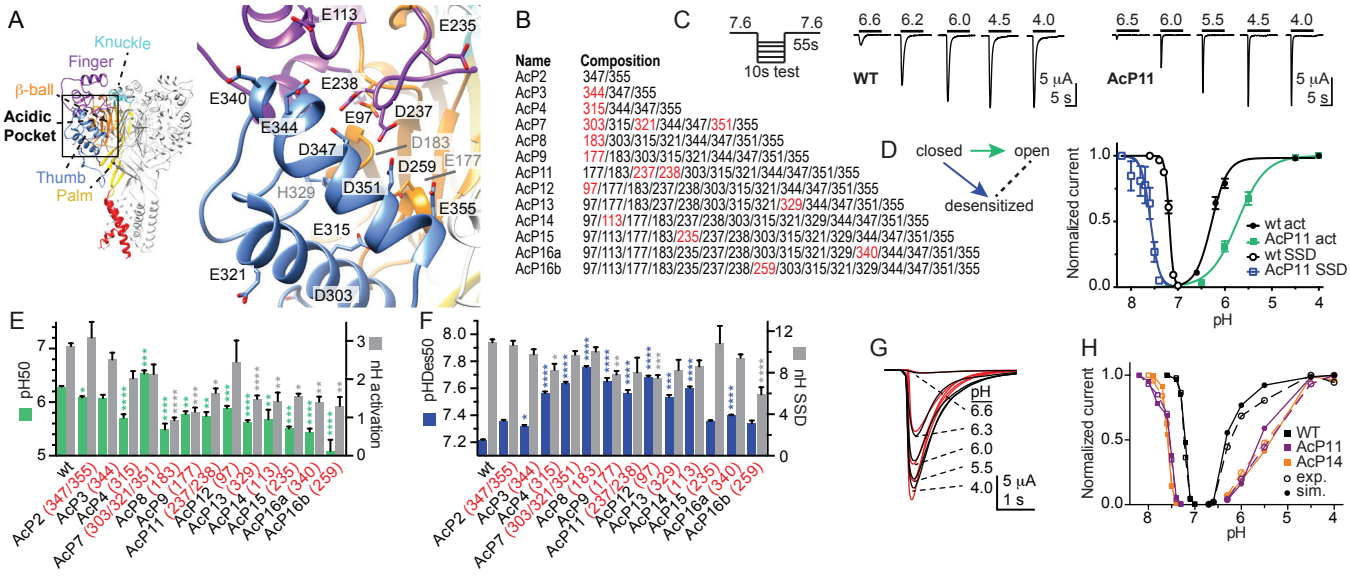
A
Knuckle
Finger
β-ball
Acidic Pocket
Thumb
Palm
E113
E235
E340
E238
E344
E97
D237
D347
D183
D259
E177
H329
D351
E355
E315
E321
D303
B
Name
Composition
AcP2 347/355
AcP3 344/347/355
AcP4 315/344/347/355
AcP7 303/315/321/344/347/351/355
AcP8 183/303/315/321/344/347/351/355
AcP9 177/183/303/315/321/344/347/351/355
AcP11 177/183/237/238/303/315/321/344/347/351/355
AcP12 97/177/183/237/238/303/315/321/344/347/351/355
AcP13 97/177/183/237/238/303/315/321/329/344/347/351/355
AcP14 97/113/177/183/237/238/303/315/321/329/344/347/351/355
AcP15 97/113/177/183/235/237/238/303/315/321/329/344/347/351/355
AcP16a 97/113/177/183/235/237/238/303/315/321/329/340/344/347/351/355
AcP16b 97/113/177/183/235/237/238/259/303/315/321/329/344/347/351/355
C
7.6
7.6
55s
10s test
6.6
6.2
6.0
4.5
4.0
WT
5 μA
5 s
6.5
6.0
5.5
4.5
4.0
AcP11
5 μA
5 s
D
closed
open
desensitized
Normalized current
1.0
0.5
0.0
8
7
6
5
4
pH
wt act
AcP11 act
wt SSD
AcP11 SSD
E
pH50
nH activation
wt
AcP2 (347/355)
AcP3 (344)
AcP4 (315)
AcP7 (303/321/351)
AcP8 (183)
AcP9 (177)
AcP11 (237/238)
AcP12 (87)
AcP13 (329)
AcP14 (113)
AcP15 (235)
AcP16a (340)
AcP16b (259)
F
pHDes50
nH SSD
G
pH
6.6
6.3
6.0
5.5
4.0
5 μA
1 s
H
Normalized current
WT
AcP11
AcP14
exp.
sim.
pH

Figure 1

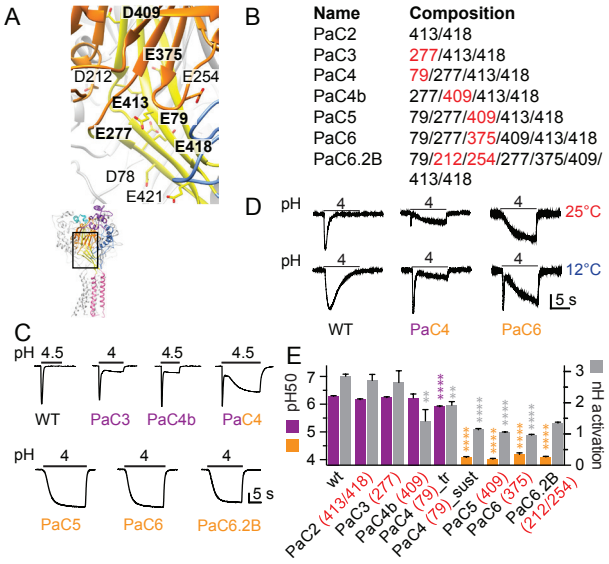
A
D409
E375
D212
E254
E413
E277
E79
E418
D78
E421
B
Name
Composition
PaC2
413/418
PaC3
277/413/418
PaC4
79/277/413/418
PaC4b
277/409/413/418
PaC5
79/277/409/413/418
PaC6
79/277/375/409/413/418
PaC6.2B
79/212/254/277/375/409/413/418
C
pH 4.5
4
4.5
4.5
WT
PaC3
PaC4b
PaC4
pH 4
4
4
5 s
PaC5
PaC6
PaC6.2B
D
pH
4
4
4
25°C
pH
4
4
4
12°C
5 s
WT
PaC4
PaC6
E
pH50
nH activation
7
6
5
4
3
2
1
0
wt
PaC2 (413/418)
PaC3 (277)
PaC4b (409)
PaC4 (79)
PaC4 (79)_lr
PaC4 (79)_sust
PaC5 (409)
PaC6 (375)
PaC6.2B (212/254)

Figure 2

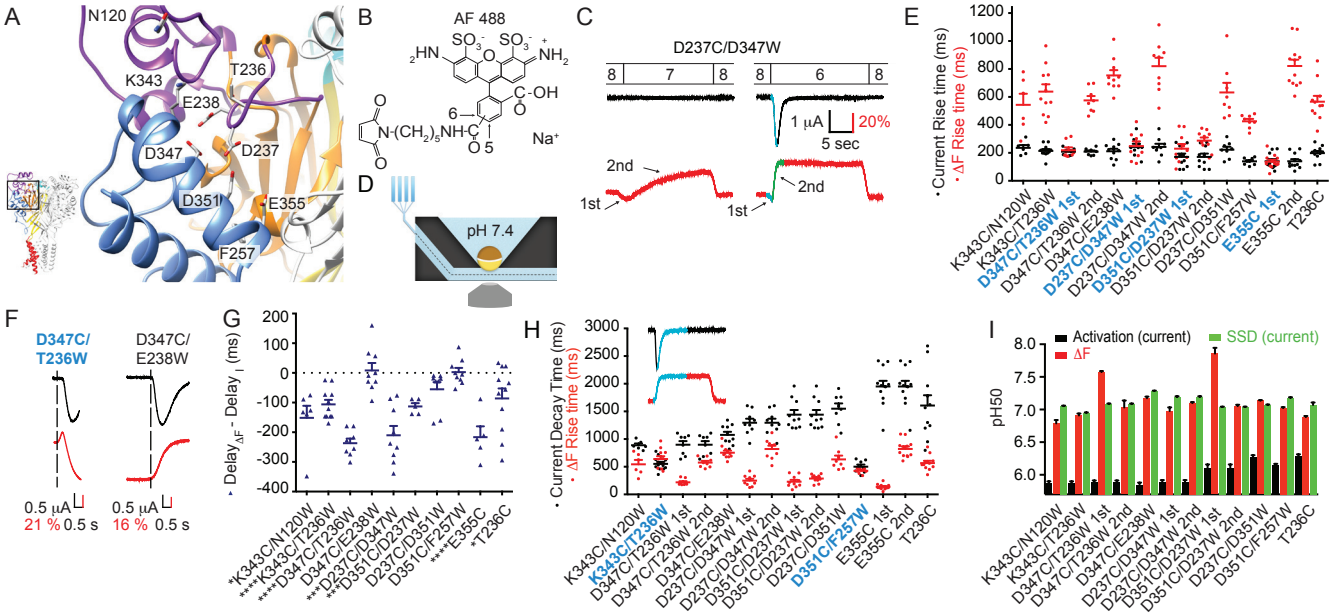
A
N120
K343
T236
E238
D347
D237
D351
E355
F257
B
AF 488
Na+
D
pH 7.4
C
D237C/D347W
1 µA
20%
5 sec
2nd
1st
E
Current Rise time (ms)
ΔF Rise time (ms)
K343C/N120W
K343C/T236W
D347C/T236W 1st
D347C/T236W 2nd
D347C/E238W
D237C/D347W 1st
D237C/D347W 2nd
D351C/D237W 1st
D237C/D237W 2nd
D351C/D351W
D351C/F257W
E355C 1st
E355C 2nd
T236C
F
D347C/ T236W
D347C/ E238W
0.5 µA
21 % 0.5 s
16 % 0.5 s
G
Delay_ΔF - Delay_I (ms)
H
Current Decay Time (ms)
ΔF Rise time (ms)
I
Activation (current)
SSD (current)
ΔF
pH50

Figure 3

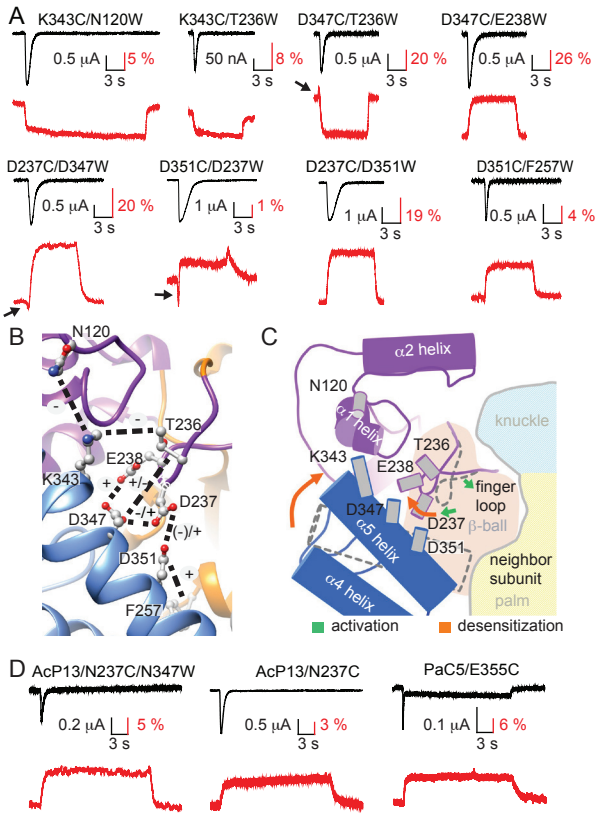
A
K343C/N120W
0.5 µA
5 %
3 s
K343C/T236W
50 nA
8 %
3 s
D347C/T236W
0.5 µA
20 %
3 s
D347C/E238W
0.5 µA
26 %
3 s
D237C/D347W
0.5 µA
20 %
3 s
D351C/D237W
1 µA
1 %
3 s
D237C/D351W
1 µA
19 %
3 s
D351C/F257W
0.5 µA
4 %
3 s
B
N120
T236
E238
K343
D237
D347
D351
F257
C
α2 helix
N120
α1 helix
knuckle
T236
K343
E238
finger
loop
β-ball
D347
α5 helix
D237
D351
neighbor
subunit
palm
α4 helix
activation
desensitization
D
AcP13/N237C/N347W
0.2 µA
5 %
3 s
AcP13/N237C
0.5 µA
3 %
3 s
PaC5/E355C
0.1 µA
6 %
3 s

Figure 4

The corresponding manuscript has been published in PNAS on March 20, 2017,
doi: 10.1073/pnas.1620560114 Link to the website: http://www.pnas.org/content/114/14/3768.long

Supporting information *Vullo et al.*

SI Methods

Molecular biology. The human ASIC1a sequence was subcloned in a pSP65-derived expression vector containing 3' and 5' non-translated sequences of *Xenopus laevis* β globin. Site-directed mutagenesis was done by using the Quikchange approach. All mutations were confirmed by sequencing (Synergen Biotech). Combined mutations were neutralization mutations, i.e. Asp to Asn, Glu to Gln, His to Asn, except for D212, that was mutated to Gly. Mutation of D212 to Asn abolished channel function (no pH 5-induced membrane current in two series of experiments). Since all other ASIC subunits contain a Gly residue at the homologous position, D212 was mutated to Gly in order to disrupt a possible protonation of this side chain. The mutant channel D212G was functional. *In vitro* transcription was carried out with the mMessage mMachine SP6 kit (Ambion/Life Technologies).

Oocyte handling and injection. All experiments with *Xenopus* were carried out in accordance with the Swiss federal law on animal welfare, following protocols that had been approved by the committee on animal experimentation of the Canton de Vaud. Oocytes were isolated and cultured as described (12). Briefly, healthy stage V and VI oocytes of female *Xenopus laevis* frogs were treated with collagenase for isolation and defolliculation. They were subsequently injected with 50-100 nl of cRNA (0.02-0.5 μg/μl). Oocytes were kept in modified Barth's saline (MBS) containing (in mM) 85 NaCl, 1 KCl, 2.4 $NaHCO_3$, 0.33 $Ca(NO_3)_2$, 0.82 $MgSO_4$, 0.41 $CaCl_2$, 10 HEPES, 4.08 NaOH. For some experiments, oocytes were kept in an MBS containing 10 mM NaCl, with 75 mM NaCl replaced by N-Methyl-D-glutamine. Oocytes that were later used for VCF were incubated after the injection during 1 h in MBS containing 10 mM 3-maleimidopropionic acid (Bachem) to modify free Cys residues of endogenous oocyte proteins at the cell surface. Measurements were done 24-56 h after injection.

Solutions and reagents. The standard recording solution was composed of (in mM) 110 NaCl, 2 $CaCl_2$, and 10 HEPES for pH values > 6.8. Solutions with a pH < 6.8 contained MES instead of HEPES. The pH was adjusted using NaOH. In some experiments NaCl was replaced by N-methyl-glucosamine (120 mM) that is not conducted by ASICs. For measurement of the current-voltage relationship, the recording solution contained (in mM) 110 NaCl, 2 $MgCl_2$ and 10 HEPES (or 10 MES for pH ≤ 6.7). To investigate the permeability to K^+ and Cs^+ ions, NaCl was substituted by the same concentration of KCl or CsCl. The pH was adjusted using NaOH,

KOH, CsOH, for solutions containing Na^+, K^+ and Cs^+, respectively. For experiments performed at different temperatures, the extracellular solution contained MOPS (which is less temperature-dependent) as pH buffer instead of HEPES or MES. 10 mM stock solutions of Alexa Fluor 488 C-5 Maleimide (AlexaFluor488, Life Technologies) and CF488A (Biotium) were prepared in DMSO and stored in aliquots at -20°C.

Electrophysiology. All experiments of the VCF part were carried out with oocytes that had been previously exposed to CF488- or Alexafluor488 maleimide. Currents were recorded by two-electrode voltage-clamp at -60 mV (-40 mV for VCF experiments) with a Dagan TEV-200 amplifier at a sampling rate of 1 ms and low-pass filtering at 2 kHz. Oocytes were impaled with two glass electrodes filled with 1 M KCl, with a resistance of < 0.8 MΩ. The perfusion speed was set to 5-15 ml/min, and switching between different solutions was controlled by electrovalves. To generate activation and steady-state desensitization (SSD) curves, the recording chamber was perfused with conditioning pH solution, and every minute ASICs were activated with stimulation solution during 5-10 s. For measurements of current-voltage relationship, the holding potential was -60 mV and 90-ms voltage ramps from -100 to +80 mV were applied every 200 ms. The conditioning pH was 7.4, the stimulation pH was 5. For experiments performed at different temperatures, the temperature of the perfusion solution was monitored in the perfusion chamber with a temperature-sensitive probe (Th-10Km, Cell MicroControls, Norfolk, USA) and changed by the perfusion solutions between 12°C and 25°C.

VCF. A total number of 30 engineered Cys-Trp pairs in the AcP were generated and tested by VCF. They had been chosen based on the following criteria: 1) the distance between their Cα atoms was ≤ 15 Å, 2) one of the residues was on the thumb helix, the other on the other side of the AcP, 3) the side chains of these residues were oriented towards each other and 4) the residue to be mutated to Cys appeared accessible from the solution as judged from the crystal structure. Only the 8 pairs whose ΔF signal was specific according to the criteria shown in table S3, and of which the corresponding Cys mutant alone did not induce a measurable ΔF, were included in the study. VCF experiments were mostly performed as described previously (33). Labeling was carried out in the dark with 5 μM CF488A maleimide or AlexaFluor488 C-5 maleimide at 19°C for 15 min. The light source was an Intensilight lamp (C-HGFI, Nikon). The emitted signal was detected by a 40x Nikon objective and quantified by a photodiode (S1336-18BQ,

Hamamatsu photonics). The ΔF was normalized to the total fluorescence intensity F, as determined with a scalable offset device. A low pass eight-pole Bessel filter was used to amplify and filter the signal at 50 Hz. On most mutants we tested the two fluorophores CF488A and AlexaFluor488. We used the one with the higher signal amplitude and better apparent specificity for the experiments. As a measure of specificity we determined the ΔF induced by acidification to pH 6 from the conditioning pH 7.4 and also from the conditioning pH of 6.8, at which the tested ASICs were desensitized and did not open. We considered the ΔF induced by the pH change from 6.8 to 6 as a potential pH effect on the fluorophore itself and determined the ratio ΔF(pH6.8→6)/ΔF(pH7.4→6) as a measure of the potentially nonspecific fraction of the signal. All mutants showed some ΔF in the pH6.8-to-6 transition, which was however generally <30% of the ΔF amplitude measured in response to the pH drop from 7.4 to 6 (Table S3). For most measurements, oocytes were placed in an RC-25 recording chamber (Warner Instruments), as described previously (33). For kinetic measurements we used a specially designed chamber to measure and compare the ΔF and current kinetics from similar oocyte surfaces (Fig. 3D). This chamber contained an upper compartment that was connected by a hole of 0.85 mm diameter to a lower channel. The oocyte was placed in the upper compartment in the hole, bathed in recording solution of pH 7.4 and was impaled with the electrodes. The bottom side of the oocyte was exposed to the lower channel, allowing the solution to flow under the oocyte, as described (35). The chamber was made based on a prototype kindly provided by G. Akk (Washington University).

Data analysis. Current recordings were controlled and recorded using Chartmaster and analyzed with Chartmaster or Fitmaster (HEKA electronics). Normalized activation curves were fitted to the Hill equation ($(I = I_{max}/(1 + (10^{-pH50}/10^{-pH})^{nH})$), where I_{max} is the maximal current, pH_{50} is the value at which the current amplitude is half-maximal and nH is the Hill coefficient (GraphPad Prism). SSD curves were fitted to an analogous equation. The kinetics of ΔF and current signals were determined as rise times, the time to get from 10 to 90% of the maximal amplitude. The permeability ratio of two ions A and B was calculated from reversal potential (E_{rev}) values determined from voltage ramps obtained when the ASIC current was induced by acidification in an extracellular solution containing either the cation A or B, from the relationship $\Delta E_{rev} = E_{rev,B} - E_{rev,A} = (RT/zF)\ln(P_B[B]_o/P_A[A]_o)$, where R, T, z and F have their usual meanings, $P_{B(or\ A)}$ is the permeability of B (or A), and $[B]_o$ and $[A]_o$ are the extracellular concentrations of ions B and A (36). Structural images were made with Chimera

(37) from a human ASIC1a homology model, based on the crystal structure of chicken ASIC1, which shares 90% sequence homology with human ASIC1a (PDB number 4NTW (8)).

Analysis of two-component ΔF signals. For mutants with two ΔF components it might be possible that under certain pH conditions the second component may decrease the apparent amplitude of the first component, which would lead to an underestimation of the rise time of the first component. This possible error was estimated and corrected as indicated in Fig. S3D-E. In the mutants with a composite ΔF signal, the pH dependence of the first component was generally shifted to alkaline values with regard to the pH dependence of the second ΔF component and reached maximal amplitudes at pH 7. This allowed observation of the first signal alone at alkaline pH values; in these mutants, saturation of the amplitude of the first ΔF component occurred at pH values at which the amplitude of the second ΔF component was still small (Fig. S3D). If at an acidic pH at which the 2^{nd} ΔF component had a high amplitude, the amplitude of the first component decreased (as illustrated in Fig. S3D), this probably indicated that the accelerated 2^{nd} component had cut a part of the first ΔF component. We observed indeed a decrease of the amplitude of the first ΔF component in the mutants D347C/T236W and D351C/D237W. This was not observed with the mutant D237C/D347W (higher ΔF amplitude at pH 6.2 than at pH 7), and it was previously shown that this is not the case for the E355C mutant (33). In principle, if this decrease in the two double mutants reflects the partial suppression of the first ΔF component by the second one, it leads to an underestimation of its rise time. We have therefore corrected the individual rise time values of the first ΔF component of these mutants measured at pH x by dividing the measured rise time by the ratio ΔF/F at pH x / ΔF/F at pH7 (Fig. S3E). An alternative would have been a double exponential fit for the two components. Due to the short duration of the first component, such fits were however not reliable.

Data presentation and statistics. Statistical comparison of two mean values was done with the t-test. For statistical analysis of more than two mean values, we determined first the distribution of the experimental population, and used for Gaussian distributions ANOVA followed by Tukey's multiple comparisons test (Graphpad Prism 6). For non-Gaussian distributions, non-parametric tests (Kruskal-Wallis, followed by Dunn's multiple comparisons test) were used. The data are presented as mean ± SEM. Individual data points and numbers of

experiments are provided in the supplemental material as an excel file. The numbers correspond to the number of individual oocytes, from which measures were taken.

Kinetic models

By using a 4-state kinetic model, we first show how mutations that mimic a protonated pH sensor affect the midpoint and the steepness of the pH-dependent state when the protonation step affected by the mutation is either 1) essential, or 2) accessory for reaching the state of interest (e.g the open state).

A second, more complex model is then used to fit the experimental data in order to better understand the mechanism underlying the observed functional effects of acidic pocket (AcP) mutations.

1) Analytic solutions for 4-state and 2-state kinetic models

We consider a 4-state kinetic model (Fig. S1C) representing a channel with 2 protonation sites (indicated by subscript *a* and superscript *b*), both of which can be protonated or not (states C, C_a, C^b and C_a^b). We use this simple 4-state model to obtain analytic expressions for the pH50 and Hill coefficient of a transition of interest (e.g. to state C_a^b) and show how these are affected by mutation at one of the two sites in two situations: 1) both protonations are essential for the transition of interest (we observe C_a^b); 2) only protonation of *b* is required for the transition of interest (we observe $C^b + C_a^b$).

Let $K_{A\to B}$ be the transition rate from state A to state B, then our model is given by:

$$K_{C\to C_a} = k_a\left(\frac{[H]}{[H_{50}^a]}\right)^{n_a} \quad ; \quad K_{C_a\to C} = k_a$$

$$K_{C\to C^b} = k_b\left(\frac{[H]}{[H_{50}^b]}\right)^{n_b} \quad ; \quad K_{C^b\to C} = k_b$$

$$K_{C_a\to C_a^b} = \alpha k_b\left(\frac{[H]}{[H_{50}^b]}\right)^{n_b} \quad ; \quad K_{C_a^b\to C_a} = k_b$$

$$K_{C^b\to C_a^b} = \alpha k_a\left(\frac{[H]}{[H_{50}^a]}\right)^{n_a} \quad ; \quad K_{C_a^b\to C^b} = k_a$$

[H] is the proton activity ($pH = -\log_{10}([H])$), $[H_{50}^a]$ is the proton activity at which proton sensor *a* is protonated in half of the channels, and similarly for $[H_{50}^b]$. n_a and n_b correspond

to the number of protons in sensors *a* and *b*, and α is the cooperativity between sensor *a* and *b* ($\alpha > 1$ corresponds to a positive cooperativity, i.e. protonation of *a* makes protonation of *b* easier, while $\alpha < 1$ corresponds to negative cooperativity). Finally k_a (respectively k_b) is the protonation rate for sensors *a* (respectively *b*) at $[H] = [H_{50}^a]$ (respectively $[H] = [H_{50}^b]$). These parameters do not influence the equilibrium state, but only the rate at which the system reaches equilibrium at a given *pH*. Note that only the forward transitions (protonation) are *pH*-dependent, just as ligand binding depends on the concentration of ligands while unbinding does not.

At equilibrium we have:

$$\begin{cases} P(C_a) = \left(\dfrac{[H]}{[H_{50}^a]}\right)^{n_a} P(C) \\ P(C^b) = \left(\dfrac{[H]}{[H_{50}^b]}\right)^{n_b} P(C) \\ P(C_a^b) = \alpha\left(\dfrac{[H]}{[H_{50}^b]}\right)^{n_b} P(C_a) \\ P(C_a^b) = \alpha\left(\dfrac{[H]}{[H_{50}^a]}\right)^{n_a} P(C^b) \\ 1 = P(C) + P(C_a) + P(C^b) + P(C_a^b) \end{cases} \qquad \text{(s1)}$$

with $P(C_x)$ = probability of the channel being in state C_x. From this system of equations (s1) we can easily obtain the equilibrium probabilities:

$$P(C) = \frac{1}{F([H])} \qquad \text{(s2)}$$

$$P(C_a) = \frac{\left(\dfrac{[H]}{[H_{50}^a]}\right)^{n_a}}{F([H])} \qquad \text{(s3)}$$

$$P(C^b) = \frac{\left(\dfrac{[H]}{[H_{50}^b]}\right)^{n_b}}{F([H])} \qquad \text{(s4)}$$

$$P(C_a^b) = \frac{\alpha\left(\dfrac{[H]}{[H_{50}^a]}\right)^{n_a}\left(\dfrac{[H]}{[H_{50}^b]}\right)^{n_b}}{F([H])} \qquad \text{(s5)}$$

with $F([H]) = 1 + \left(\frac{[H]}{[H_{50}^a]}\right)^{n_a} + \left(\frac{[H]}{[H_{50}^b]}\right)^{n_b} + \alpha\left(\frac{[H]}{[H_{50}^a]}\right)^{n_a}\left(\frac{[H]}{[H_{50}^b]}\right)^{n_b}$ (s6)

For the remainder of this section we will assume that both transitions correspond to single protonation sites ($n_a = 1$ and $n_b = 1$). Let us first consider the case where both protonations are needed for the transition of interest, so we define $[H_{50}]_{4state}$ as the proton concentration at which half the channels have both sites protonated $P(C_a^b, [H_{50}]_{4state}) = 1/2$. It follows from equation s5 that:

$$[H_{50}]_{4state} = \frac{[H_{50}^a] + [H_{50}^b] + \sqrt{([H_{50}^a] + [H_{50}^b])^2 + 4\alpha[H_{50}^a][H_{50}^b]}}{2\alpha} > \frac{[H_{50}^a] + [H_{50}^b]}{\alpha} \quad \text{(s6)}$$

The Hill coefficient for this transition ($C \rightarrow C_a^b$) is given by:

$$n_{4state} = \frac{d}{d\log([H])}\log\left(\frac{P(C_a^b)}{1 - P(C_a^b)}\right)\Bigg|_{[H]=[H_{50}]}$$

$$= [H]\frac{d}{d[H]}\log\left(\frac{\alpha[H][H]}{[H_{50}^a][H_{50}^b] + [H]([H_{50}^a] + [H_{50}^b])}\right)\Bigg|_{[H]=[H_{50}]}$$

$$= \frac{[H]}{\alpha[H][H]}\left(2\alpha[H] - \frac{\alpha[H][H]([H_{50}^a] + [H_{50}^b])}{[H_{50}^a][H_{50}^b] + [H]([H_{50}^a] + [H_{50}^b])}\right)\Bigg|_{[H]=[H_{50}]}$$

$$= 2 - \frac{[H]([H_{50}^a] + [H_{50}^b])}{[H_{50}^a][H_{50}^b] + [H]([H_{50}^a] + [H_{50}^b])}\Bigg|_{[H]=[H_{50}]}$$

$$= 1 + \frac{[H_{50}^a][H_{50}^b]}{[H_{50}^a][H_{50}^b] + [H]([H_{50}^a] + [H_{50}^b])}\Bigg|_{[H]=[H_{50}]} > 1 \quad \text{(s7)}$$

Let us now consider how the pH_{50} and n would be affected by a neutralization mutation of one of the two protonation sites. For this, we consider that a neutralization mutation corresponds to one of the sites being always protonated (in this example the site "a"), so that we are left with a two-state model (states C_a and C_a^b) for which it is easy to show that

$$P_{2state}(C_a^b) = \frac{\alpha\left(\frac{[H]}{[H_{50}^b]}\right)^{n_b}}{1 + \alpha\left(\frac{[H]}{[H_{50}^b]}\right)^{n_b}} \quad \text{(s8)}$$

$$[H_{50}]_{2state} = \frac{[H_{50}^b]}{\alpha} \quad \text{(s9)}$$

$$n_{2state} = 1 \qquad \text{(s10)}$$

From the comparison of equations (s6) with (s9) and (s7) with (s10), it is clear that:

$$[H_{50}]_{4state} > [H_{50}]_{2state} \Rightarrow pH50_{4state} < pH50_{2state}$$

$$n_{4state} > n_{2state}$$

so that in this model (two protonation sites, both needed for the transition of interest), a protonation-mimicking mutation will always increase the *pH50* while decreasing the Hill coefficient. This is exemplified in Fig. S1D showing simulated data with such a 4-state model (red triangles and lines) and the impact of a neutralization mutation (black circles and line).

If instead we consider the first protonation ("a") as accessory to the transition of interest brought about by the second protonation (i.e. that in this case, both, C^b and C_a^b are "states of interest") we get for the 4-state model:

$$P(C_a^b, [H_{50}]_{4state}^{accessory}) + P(C^b, [H_{50}]_{4state}^{accessory}) = 1/2$$

$$[H_{50}]_{4state}^{accessory} = \frac{[H_{50}^a] - [H_{50}^b] + \sqrt{([H_{50}^a] - [H_{50}^b])^2 + 4\alpha[H_{50}^a][H_{50}^b]}}{2\alpha}$$

Let us now show that $[H_{50}]_{4state}^{accessory}$ can be both smaller and larger than $[H_{50}]_{2state}$, which is equivalent to the ratio $\frac{[H_{50}]_{4state}^{accessory}}{[H_{50}]_{2state}}$ being either smaller or larger than 1.

$$\frac{[H_{50}]_{4state}}{[H_{50}]_{2state}} = \frac{\alpha[H_{50}]_{4state}}{[H_{50}^b]} = \frac{1}{2}\left[\left(\frac{[H_{50}^a]}{[H_{50}^b]} - 1\right) + \sqrt{\left(\frac{[H_{50}^a]}{[H_{50}^b]} - 1\right)^2 + 4\alpha\frac{[H_{50}^a]}{[H_{50}^b]}}\right] \qquad \text{(s11)}$$

Equation s11 is plotted in Fig. S1E as a function of $\frac{[H_{50}^a]}{[H_{50}^b]}$ and α, clearly showing that $[H_{50}]_{4state}^{accessory}$ can be larger (red region in Fig. S1E) or smaller (blue region in Fig. S1E) than $[H_{50}]_{2state}$. This proves that a protonation-mimicking mutation of a site that is accessory to the transition of interest can either decrease or increase the *pH50*.

Similarly, we now calculate the Hill coefficient in the case of protonation *a* being accessory to the observed transition (transition to $C^b + C_a^b$). In this case the Hill coefficient is defined as:

$$n_{4state}^{accessory} = \frac{d}{d\log([H])}\log\left(\frac{P_{C_a^b}+P_{C^b}}{1-P_{C_a^b}-P_{C^b}}\right)\Bigg|_{[H]=[H_{50}]}$$

$$=[H]\frac{d}{d[H]}\log\left(\frac{\alpha[H][H]+[H_{50}^b][H]}{[H_{50}^a][H_{50}^b]+[H][H_{50}^a]}\right)\Bigg|_{[H]=[H_{50}]}$$

$$=\frac{[H]}{\alpha[H][H]+[H_{50}^b][H]}\left(2\alpha[H]+[H_{50}^b]-\frac{(\alpha[H][H]+[H_{50}^b][H])[H_{50}^a]}{[H_{50}^a][H_{50}^b]+[H][H_{50}^a]}\right)\Bigg|_{[H]=[H_{50}]}$$

$$=1+\frac{\alpha[H][H]}{\alpha[H][H]+[H_{50}^b][H]}-\frac{[H][H_{50}^a]}{[H_{50}^a][H_{50}^b]+[H][H_{50}^a]}\Bigg|_{[H]=[H_{50}]}$$

$$=1+\frac{\alpha[H][H]\left([H_{50}^a][H_{50}^b]+[H][H_{50}^a]\right)-[H][H_{50}^a]\left(\alpha[H][H]+[H_{50}^b][H]\right)}{\left(\alpha[H][H]+[H_{50}^b][H]\right)\left([H_{50}^a][H_{50}^b]+[H][H_{50}^a]\right)}\Bigg|_{[H]=[H_{50}]}$$

$$=1+\frac{[H_{50}^a][H_{50}^b][H][H](\alpha-1)}{\left(\alpha[H][H]+[H_{50}^b][H]\right)\left([H_{50}^a][H_{50}^b]+[H][H_{50}^a]\right)}\Bigg|_{[H]=[H_{50}]} \quad \text{(s12)}$$

Note that the second term in equation (s12) will be positive for $\alpha>1$ and negative for $\alpha<1$ (α is always positive, so the denominator is always positive). So it is clear that a mutation mimicking the protonation of an accessory site will lead to a decrease in Hill coefficient for positive cooperativity (if $\alpha>1$ then $n_{4state}^{accessory}>1=n_{2state}$), and an increase in Hill coefficient in case of negative cooperativity (if $\alpha<1$ then $n_{4state}^{accessory}<1=n_{2state}$). These results are exemplified in Fig. S1D showing the equilibrium probabilities for such a 4-state model (blue triangles and lines) and the impact of a neutralization mutation on its pH50 and Hill coefficient (black circles and line), thus illustrating that the pH50 shift of such a mutation can be alkaline or acidic.

2) Kinetic model for fitting experimental ASIC1a data

2a) Model in which protonation of the AcP is accessory for activation and desensitization

The kinetic model of ASIC1a, illustrated in Fig. S1F, is composed of 32 states corresponding to 3 sets of protonation sites (o=activation, d=desensitization and a=acidic pocket) and 4 conformations (C=closed, O=open, D=closed-desensitized and OD=open-desensitized). For computational reasons (see below), the protonation of closed channels towards opening and desensitization is represented by two steps each ($C\rightarrow C^o\rightarrow C^O$, $C\rightarrow C^d\rightarrow C^D$), which does not mean that exactly two protonation steps are involved. Opening and desensitization involve a final pH-independent transition ($C^O\rightarrow O^O$, $C^D\rightarrow D^D$). Evidence for such a ligand-independent transition before opening comes from several studies with ligand-gated ion channels (38, 39).

Each of these 16 states can exist with the proton sensor in the AcP protonated or not (e.g. C and ^{a}C), yielding a total of 32 states.

Protonation transitions are described by their pH50 (or the equivalent proton concentration [H_{50}]) at which the protonation and deprotonation rates are equal, the Hill coefficient n, and their transition rate at pH=pH50, k. For example protonation of the AcP

$$K_{C\to {}^{a}C} = k_a \left(\frac{[H]}{[H_{50}^{a}]} \right)^{n_a} = k_a 10^{-n_a (pH - pH_{50}^{a})} \qquad \text{(s13)}$$

while the reverse transition is given by

$$K_{{}^{a}C\to C} = k_a$$

Similar expressions were also used for the protonations of activation and desensitization sites, except that these transitions were split into two identical transitions (C $\rightarrow$C^{o} $\rightarrow$ C^{O}, C $\rightarrow$C^{d} $\rightarrow$C^{D}). This was done because these transitions have large Hill coefficients (We found values of ~11 for desensitization and 3 for activation), which led to difficulties in the simulation. Splitting these transitions decreases the corresponding Hill coefficient by a factor of 2, which allowed for easier integration of the equations.

$$K_{C\to C_d} = k_d 10^{-n_d (pH - pH_{50}^{d})} \quad ; \quad K_{C_d\to C} = k_d \qquad \text{(s14)}$$

$$K_{C_d\to C_D} = k_d 10^{-n_d (pH - pH_{50}^{d})} \quad ; \quad K_{C_D\to C_d} = k_d$$

$$K_{C\to C^o} = k_o 10^{-n_o (pH - pH_{50}^{o})} \quad ; \quad K_{C^o\to C} = k_o \qquad \text{(s15)}$$

$$K_{C^o\to C^O} = k_o 10^{-n_o (pH - pH_{50}^{o})} \quad ; \quad K_{C^O\to C^o} = k_o$$

The rates of the pH-independent transitions to the open and desensitized states are

$$K_{C^o\to O^o} = f_O \quad ; \quad K_{O^o\to C^o} = b_O \qquad \text{(s16)}$$

$$K_{C_D\to D_D} = f_D \quad ; \quad K_{D_D\to C_D} = b_D \qquad \text{(s17)}$$

We included cooperativity between protonation of the AcP and the other protonations, as well as with channel opening and desensitization.

$$K_{{}^{a}C\to {}^{a}C_d} = \alpha_D K_{C\to C_d} \qquad \text{(s18)}$$

$$K_{{}^{a}C\to {}^{a}C^o} = \alpha_O K_{C\to C^o} \qquad \text{(s19)}$$

$$K_{{}^{a}C_D \to {}^{a}D_D} = \beta_D K_{C_D \to D_D} \qquad \text{(s20)}$$

$$K_{{}^{a}C^O \to {}^{a}O^O} = \beta_O K_{C^O \to O^O} \qquad \text{(s21)}$$

The 4 cooperativity parameters (α_D, α_O, β_D and β_O) are always positive, with values below 1 indicating negative cooperativity (e.g if $\alpha_D < 1$, protonation of AcP will make the protonation of the desensitization sites harder), and values above 1 corresponding to positive cooperativity (e.g if $\alpha_D > 1$, protonation of AcP will make the protonation of the desensitization sites easier). To respect microscopic reversibility this also leads to cooperativity between the other transitions and protonation of the AcP

$$K_{C_d \to {}^{a}C_d} = \alpha_D K_{C \to {}^{a}C} \quad ; \quad K_{C_D \to {}^{a}C_D} = \alpha_D \alpha_D K_{C \to {}^{a}C}$$

$$K_{C_o \to {}^{a}C_o} = \alpha_O K_{C \to {}^{a}C} \quad ; \quad K_{C_O \to {}^{a}C_O} = \alpha_O \alpha_O K_{C \to {}^{a}C}$$

$$K_{C_d^o \to {}^{a}C_d^o} = \alpha_D \alpha^O K_{C \to {}^{a}C} \; ; \quad K_{C_D^o \to {}^{a}C_D^o} = \alpha_D \alpha_D \alpha^O K_{C \to {}^{a}C}$$

$$K_{C_d^O \to {}^{a}C_d^O} = \alpha_D \alpha^O \alpha^O K_{C \to {}^{a}C} \quad ; \quad K_{C_D^O \to {}^{a}C_D^O} = \alpha_D \alpha_D \alpha^O \alpha^O K_{C \to {}^{a}C}$$

$$K_{D_D \to {}^{a}D_D} = \alpha_D \alpha_D \beta_D K_{C \to {}^{a}C} \; ; \; K_{D_D^o \to {}^{a}D_D^o} = \alpha_O \alpha_D \alpha_D \beta_D K_{C \to {}^{a}C} \; ; \; K_{D_D^O \to {}^{a}D_D^O} = \alpha_O \alpha_O \alpha_D \alpha_D \beta_D K_{C \to {}^{a}C}$$

$$K_{O^O \to {}^{a}O^O} = \alpha_O \alpha_O \beta^O K_{C \to {}^{a}C} \; ; \; K_{O_d^O \to {}^{a}O_d^O} = \alpha_D \alpha_O \alpha_O \beta^O K_{C \to {}^{a}C} \; ; \; K_{O_D^O \to {}^{a}O_D^O} = \alpha_D \alpha_D \alpha_O \alpha_O \beta^O K_{C \to {}^{a}C}$$

$$K_{OD_D^O \to {}^{a}OD_D^O} = \alpha_O \alpha_O \alpha_D \alpha_D \beta_D \beta^O K_{C \to {}^{a}C}$$

The remaining rates are all equivalent to one of the rates defined above. For the reverse reactions all rates for reactions shown with the same color in Fig. S1F are identical:

$$K_{{}^{a}C_d \to C_d} = K_{{}^{a}C_D \to C_D} = K_{{}^{a}C^o \to C^o} = K_{{}^{a}C^O \to C^O} = K_{{}^{a}C_d^o \to C_d^o} = K_{{}^{a}C_D^o \to C_D^o} = K_{{}^{a}C_d^O \to C_d^O} = K_{{}^{a}C_D^O \to C_D^O} = K_{{}^{a}C \to C}$$

$$K_{{}^{a}O^O \to O^O} = K_{{}^{a}O_d^O \to O_d^O} = K_{{}^{a}O_D^O \to O_D^O} = K_{{}^{a}C \to C}$$

$$K_{{}^{a}D_D \to D_D} = K_{{}^{a}D_D^o \to D_D^o} = K_{{}^{a}D_D^O \to D_D^O} = K_{{}^{a}OD_D^O \to OD_D^O} = K_{{}^{a}C \to C}$$

$$K_{C_d^o \to C^o} = K_{C_d^O \to C^O} = K_{O_d^O \to O^O} = K_{{}^{a}C_d^o \to {}^{a}C^o} = K_{{}^{a}C_d^O \to {}^{a}C^O} = K_{{}^{a}O_d^O \to {}^{a}O^O} = K_{{}^{a}C_d \to {}^{a}C} = K_{C_d \to C}$$

$$K_{C_D^o \to C_d^o} = K_{C_D^O \to C_d^O} = K_{O_D^O \to O_d^O} = K_{{}^{a}C_D^o \to {}^{a}C_d^o} = K_{{}^{a}C_D^O \to {}^{a}C_d^O} = K_{{}^{a}O_D^O \to {}^{a}O_d^O} = K_{{}^{a}C_D \to {}^{a}C_d} = K_{C_D \to C_d}$$

$$K_{{}^{a}D_D \to {}^{a}C_D} = K_{D_D^o \to C_D^o} = K_{D_D^O \to C_D^O} = K_{{}^{a}D_D^o \to {}^{a}C_D^o} = K_{{}^{a}D_D^O \to {}^{a}C_D^O} = K_{OD_D^O \to O_D^O} = K_{{}^{a}OD_D^O \to {}^{a}O_D^O} = K_{D_D \to C_D}$$

$$K_{C_d^o \to C_d} = K_{C_D^o \to C_D} = K_{D_D^o \to D_D} = K_{{}^{a}C^o \to {}^{a}C} = K_{{}^{a}C_d^o \to {}^{a}C_d} = K_{{}^{a}C_D^o \to {}^{a}C_D} = K_{{}^{a}D_D^o \to {}^{a}D_D} = K_{C^o \to C}$$

$$K_{C_d^O \to C_d^o} = K_{C_D^O \to C_D^o} = K_{D_D^O \to D_D^o} = K_{{}^{a}C^O \to {}^{a}C^o} = K_{{}^{a}C_d^O \to {}^{a}C_d^o} = K_{{}^{a}C_D^O \to {}^{a}C_D^o} = K_{{}^{a}D_D^O \to {}^{a}D_D^o} = K_{C^O \to C^o}$$

$$K_{O_d^O \to C_d^O} = K_{O_D^O \to C_D^O} = K_{OD_D^O \to D_D^O} = K_{{}^aO^O \to {}^aC^O} = K_{{}^aO_d^O \to {}^aC_d^O} = K_{{}^aO_D^O \to {}^aC_D^O} = K_{{}^aOD_D^O \to {}^aD_D^O} = K_{O^O \to C^O}$$

For the forward rates, this is not the case because of cooperativity and we have:

$$K_{C^o \to C_d^o} = K_{C^O \to C_d^O} = K_{O^O \to O_d^O} = K_{C_d \to C_D} = K_{C_d^o \to C_D^o} = K_{C_d^O \to C_D^O} = K_{O_d^O \to O_D^O} = K_{C \to C_d}$$

$$K_{{}^aC^o \to {}^aC_d^o} = K_{{}^aC^O \to {}^aC_d^O} = K_{{}^aO^O \to {}^aO_d^O} = K_{{}^aC_d \to {}^aC_D} = K_{{}^aC_d^o \to {}^aC_D^o} = K_{{}^aC_d^O \to {}^aC_D^O} = K_{{}^aO_d^O \to {}^aO_D^O} = K_{{}^aC \to {}^aC_d}$$

$$K_{C_D^o \to D_D^o} = K_{C_D^O \to D_D^O} = K_{O_D^O \to OD_D^O} = K_{C_D \to D_D}$$

$$K_{{}^aC_D^o \to {}^aD_D^o} = K_{{}^aC_D^O \to {}^aD_D^O} = K_{{}^aO_D^O \to {}^aOD_D^O} = K_{{}^aC_D \to {}^aD_D}$$

$$K_{C_d \to C_d^o} = K_{C_D \to C_D^o} = K_{D_D \to D_D^o} = K_{C_d^o \to C_d^O} = K_{C_D^o \to C_D^O} = K_{D_D^o \to D_D^O} = K_{C^o \to C^O} = K_{C \to C^o}$$

$$K_{{}^aC_d \to {}^aC_d^o} = K_{{}^aC_D \to {}^aC_D^o} = K_{{}^aD_D \to {}^aD_D^o} = K_{{}^aC^o \to {}^aC^O} = K_{{}^aC_d^o \to {}^aC_d^O} = K_{{}^aC_D^o \to {}^aC_D^O} = K_{{}^aD_D^o \to {}^aD_D^O} = K_{{}^aC \to {}^aC^o}$$

$$K_{C_d^O \to O_d^O} = K_{C_D^O \to O_D^O} = K_{D_D^O \to OD_D^O} = K_{C^O \to O^O}$$

$$K_{{}^aC_d^O \to {}^aO_d^O} = K_{{}^aC_D^O \to {}^aO_D^O} = K_{{}^aD_D^O \to {}^aOD_D^O} = K_{{}^aC^O \to {}^aO^O}$$

The current is defined from the fraction of channels in an open state and the conductance of the channels as

$$I = G \times (O^O + O_d^O + O_D^O + {}^aO^O + {}^aO_d^O + {}^aO_D^O)$$

Voltage and ion concentrations were the same for all experiments and were therefore not explicitly modeled (absorbed in the conductance G).

Fit of the kinetic models to the experimental data

The 32 state kinetic model of ASIC comprised 17 free parameters, 3 for protonation of the AcP (pH_{50}^a, n_a and k_a, see eq. s13), 3 for the protonation of the activation sites (pH_{50}^o, n_o and k_o, see eq. s14) and 3 for the protonation of the desensitization sites (pH_{50}^d, n_d and k_d, see eq. s15), 1 for each of channel opening, closing, desensitization, and recovery (f_O, b_O, f_D, and b_D, equations s16 and s17) and 4 cooperativity coefficients (α_O, α_D, β_O, β_D equations s18, s19, s20 and s21).

Each mutant was described by 3 parameters, each changing one of the parameters describing the protonation of the AcP:

$pH_{50}^a \Rightarrow pH_{50}^a + \Delta pH_{50}^a$ with $\Delta pH_{50}^a > 0$

$n_d \Rightarrow \varepsilon \times n_d$ with $0 < \varepsilon < 1$

$k_d \Rightarrow \gamma \times k_d$

As we fitted the model to data for the WT channel and two mutants, this added 6 parameters. Finally, the data used came from 6 different cells (one for activation and one for desensitization for the WT and both mutant channels), which added 6 parameters describing the overall conductance of ASICs for each cell. This gave a total of 29 free parameters.

The model was fit to measured currents from the activation (step from conditioning pH to different acidic pH, see Fig. 1C) and desensitization protocols (step from different conditioning pH to an acidic pH, blue arrow in Fig. 1D). Specifically we used currents from 7 activation and 6 desensitization steps for the WT, 5 activation and 8 desensitization steps for the AcP11 mutant and 7 activation and 6 desensitization steps for the AcP14 mutant. The model was fitted to all the traces simultaneously, using the Data2Dynamics software (34) with a deterministic optimization procedure repeated more than 50 times from different starting parameter obtained from a latin hypercube sampling (40).

2b) Kinetic Model with protonation of AcP essential for Activation or Desensitization

The above model was modified to describe a situation where protonation of the AcP is an essential component of either activation or desensitization, i.e. the channel can only activate or desensitize if the AcP is protonated. In the former case, this was simply represented by removing the open states without the AcP protonated (O^O, O_d^O, O_D^O and OD_D^O) while for the latter (AcP essential for desensitization) we removed the desensitized states without AcP protonated (D_D, D_D^o, D_D^O and OD_D^O).

Supplementary figure legends

Fig. S1. ASIC modeling and properties of acidic pocket mutants. *(A)* desensitization kinetics of acidic pocket mutants. The current decay phase of ASIC currents was fitted to a single exponential; n=3-19. The red numbers in the labels indicate the residues mutated in addition to the mutations already present in the preceding mutant (with a lower number of mutations; generally on the left). *(B)* sustained current / peak current amplitude (I_{sust}/I_{peak}) ratio of acidic pocket mutants determined at pH 5, 4.5 and 4, as indicated, n=3-18. *(C)* and *(D)* Illustration of the effect of a neutralization mutation on the pH50 and Hill coefficient in a 4-state model with two protonation sites *(C)*. The neutralization mutation is modeled as one of the sites being always protonated and corresponds to a 2-state kinetic model. Results for

the 2 state models (corresponding to the mutant) were obtained from equation s8 (*SI Methods*) and are shown as black circles, to which a Hill function was fitted (black line) yielding a pH50=7.0 and Hill coefficient n=1. WT channels correspond to a 4-state model (equations s2-5) with one of the protonation transitions (transition *a* in the equations) having the exact same parameters as in the 2-state model (black circles). If both protonations are essential for the observed transition, the state of interest is C_a^b , therefore we plot $P(C_a^b)$ obtained from equation s5. In this case WT channels (red triangles) have lower pH50 and higher (or equal) Hill coefficient than the mutant (black circles), both for positive (red upward triangles) and negative cooperativity between the two protonation sites (red downward triangles). As before, pH50 and Hill coefficients were obtained from the fit of a Hill function (red lines). Finally, if protonation *a* is accessory to the transition of interest (protonation *b; (D),* NE = not essential), the states of interest correspond to C_a^b and C^b, therefore we plot $P(C^b)+P(C_a^b)$ (blue triangles) obtained from equations s4 and s5. In this case, the WT channel can have a pH50 that is either larger (downward blue triangles) or smaller (upward blue triangles) than the mutant channel. Note that, as shown analytically in eq. s12, the Hill coefficient of the WT channel is smaller (respectively larger) than that of the mutant for negative (respectively positive) cooperativity. *(E)* $\frac{[H_{50}]_{4state}^{accessory}}{[H_{50}]_{2state}}$ (i.e. the ratio of the $[H_{50}]$ of the 4-state model where protonation of site *a* is accessory vs the $[H_{50}]$ of the mutant in which site *a* has been mutated to a residue mimicking protonation), is shown as a function of $\frac{[H_{50}^a]}{[H_{50}^b]}$ and α (eq. s11). Red regions indicate $[H_{50}]_{4state}^{accessory} > [H_{50}]_{2state}$ (pH_{50} is increased by the mutation) and blue $[H_{50}]_{4state}^{accessory} < [H_{50}]_{2state}$ (pH_{50} is decreased by the mutation). *(F)* Model used for fitting experimental traces of WT, AcP11 and AcP14 activation and SSD, as described in *SI Methods*. The model is composed of 32 states corresponding to 3 sets of protonation sites (o=activation, d=desensitization and a=acidic pocket) and 4 conformations (C=closed, O=open, D=desensitized and OD=open desensitized).

Fig. S2. Properties of palm mutants. *(A)* I_{sust}/I_{peak} ratio of combined palm mutants; n=3-18. *(B)* The I_{peak}/I_{sust} ratio is plotted for WT, PaC4 and PaC6 at the indicated temperatures. Data were recorded at pH 4 from a conditioning pH of 7.4 (n=7-10). *(C)* I_{sust}/I_{peak} ratio of single palm mutants, n=4-28. Mutations to Cys of E79 and E421 have been shown to induce a

I_{sust}/I_{peak} ratio of 5 ± 1 % and 1 ± 1%, respectively (21). For bar graphs of I_{sust}/I_{peak} note that for some mutants the I_{sust}/I_{peak} ratio was not measured at all three pH values. *(D-G)* current-voltage relationship of ASIC1a WT-I_{peak} *(D),* PaC4-I_{peak} *(E),* PaC4-I_{sust} *(F)* and PaC6-I_{sust} *(G)* in presence of either Na^+ (red), K^+ (blue) or Cs^+ (green) in the extracellular solution. The holding potential was -60 mV and 90-ms voltage ramps from -100 to +80 mV were applied. The pH 5-induced ramp current was calculated as the difference between the ramp current obtained during the acidification (during the peak or the sustained phase) and the ramp current measured during the conditioning period at pH 7.4. For each cell, the pH 5-induced currents with extracellular Na^+, K^+ and Cs^+-containing solution were normalized to the amplitude measured with Na^+ at -80 mV. Dotted lines represent SEM of independent experiments (n=3-11). *(H)* pH 5.5-induced current as function of amiloride concentration, normalized to the control condition. IC_{50} values obtained from the fits were 125 ± 43 μM (WT-I_{peak}) and 65 ± 13 μM (PaC4-I_{peak}), n=6. *(I)* Effect of 1 mM amiloride on WT and mutant currents as indicated. The $I_{amiloride}/I_{control}$ ratio obtained at pH 5.5 is shown, n=6-8. *(J)* Structural image showing residues pointing to the wrist that were mutated. Note that D78 is oriented towards H73 of a neighboring subunit. *(K)* Representative current traces of palm mutants in which residues H73, D78 and/or E421 were mutated in the background of various PaC mutants. H73 was mutated to Ala or Lys, since mutation to Asn resulted in very small currents. The vertical bar corresponds to the following current amplitude in μA: 0.6 (PaC4+78), 0.5 (PaC4+73A+78), 0.45 (PaC4+73K+78), 5 (PaC5+78), 2 (PaC6+78), 0.6 (PaC6.2B+78), 0.2 (PaC6.2B+421) and 1 (PaC6.2B+78+421). The color of the label refers, as the color of bars in panels *L-N*, to the PaC mutant on which the mutant is based. *(L)* I_{sust}/I_{peak} of the indicated mutants, n=6-28. *(M, N)* pH50 and nH of activation of palm-wrist mutants, n=6-129. The color indicates the palm mutant on which the mutant is based, the pattern refers to the added mutations. Statistically significant difference to WT or the corresponding palm mutant on which palm-wrist mutants are based (*M, N*; i.e. PaC4+78 is compared to PaC4_tr, etc.), are indicated as *, $p<0.05$, **, $p<0.01$, ***, $p<0.001$ and ****, $p<0.0001$. For A, C and L, all values close to 1 and higher were different from the WT I_{sust}/I_{peak}, for other values as indicated.

Fig. S3. VCF experiments of the acidic pocket. *(A)* Left, close-up view of the acidic pocket showing the residues of pairs that gave rise to fluorescence signals. Right, distances (Å)

between the C-*alpha* atoms of the corresponding residues, measured in homology models of the open (4NTW (8)) and desensitized structures (4NYK (6)). *(B)* Current and ΔF kinetics at various stimulation pH conditions. Comparison of current activation and ΔF kinetics of selected mutants measured at different pH, n=3-12. ΔF and current signals were correlated (Table S2) in all conditions except pH5.5 for D347C/T236W^{1st} and pH6.3 for E355C^{1st}. *(C)* Representative current (black) and fluorescence (red) traces of triple mutants in response to extracellular acidification to pH 6. They represent the double mutants used in the VCF part of the study, in which in addition the mutation W233V was introduced to verify that this nearby Trp residue had not influenced the ΔF signals. The conditioning pH for these experiments was 7.4. The traces are representative of 4-9 oocytes. Note that all these mutants gave consistent ΔF and current signals, except for D351C/F257W/W233V which produced small signals that were not present in all oocytes tested.

(D-E) possible errors in the measurement of the kinetics of ΔF signals containing two components, and correction of the rise time values. *(D)* representative ΔF traces of the D347C/T236W mutant obtained under different pH changes, to illustrate the overlap of the negative ΔF component over the positive component at more acidic pH conditions. *(E)* ΔF amplitude ratio of the 1st ΔF component at the indicated pH / its amplitude at pH 7 (where the signal was maximal), n=6-21. These ratios were used to correct the rise time values as indicated in *S.I. Methods*.

Fig. S4. Combined neutralization and VCF mutations. The figure shows pH and kinetic parameters of the combined mutants AcP13/N237C/N347W and PaC5/E355C (red and black symbols and bars) and compares them to these mutants in the WT background, D237C/D347W and E355C (grey and faintly colored symbols and bars). *(A,B)* pH50 and nH of current activation (black and grey) and ΔF (red tones) of the Cys and Cys/Trp mutants combined with the mutant AcP13 or PaC5, compared to values obtained with the Cys and Cys/Trp mutants alone (n= 4-7). *(C)* Current and ΔF rise time, *(D)* Current decay time and ΔF rise time and *(E)* $Delay_{\Delta F}$-$Delay_I$ of the same mutants (n=5-12). *, $p<0.05$; **,$p<0.01$; ***, $p<0.001$ and ****, $p<0.0001$ for the comparison between AcP13/N237C/N347W and D237C/D347W, and between PaC5/E355C and E355C; for mutants with two ΔF components, only the kinetics of the second ΔF components were compared.

Table S1. ΔF/F amplitude of mutants

Mutant	Ratio ΔF/F amplitude (%)	n
D237C[C]	-6.83 ± 2.13	8
D351C[C]	0.4 ± 0.92	5
K343C	1.20 ± 0.43	4
K343C[C]	0.3 ± 0.05	3
D347C	1.08 ± 0.31	8
T236C	37.89 ± 6.78	8
E355C	7.27 ± 1.25	3
K343C/N120W[C]	-8.07 ± 1.22	6
K343C/T236W	-8.48 ± 2.74	3
D347C/T236W	-7.80 ± 2.43	4
D347C/E238W	39.94 ± 19.88	3
D237C/D347W[C*]	22.56 ± 12.17	6
D351C/D237W[C]	6.51 ± 1.28	6
D351C/F257W[C]	9.36 ± 1.15	5
D237C/D351W[C]	16.63 ± 4.87	7
AcP13/N237C	7.91 ± 0.68	4
AcP13/N237C/N347W	8.13 ± 1.27	13
PaC5/E355C	8.58 ± 1.41	11

The absolute ΔF/F values, obtained at pH 6, are indicated. Mutant channels were labeled with Alexa Fluor 488, except where indicated with "C", in which case channels were labeled with CF488A. *, pH 6.2 instead of 6 in 4 of 6 experiments.

Table S2. Steepness factor of linear regression of kinetics

Mutant	pH	Steepness Factor
A. rise time$_{\Delta F}$ vs. rise time$_{current}$ at pH6		
K343C/N120W		2.30 ± 0.27
K343C/T236W		2.91 ± 0.27
D347C/T236W 1st		**1.05 ± 0.08**
D347C/T236W 2nd		2.73 ± 0.17
D347C/E238W		3.45 ± 0.18
D237C/D347W 1st		**1.03 ± 0.08**
D237C/D347W 2nd		3.15 ± 0.39
D351C/D237W 1st		**1.28 ± 0.15**
D351C/D237W 2nd		1.43 ± 0.23
D351C/F257W		3.00 ± 0.16
D237C/D351W		2.72 ± 0.34
E355C 1st		**0.90 ± 0.11**
E355C 2nd		5.11 ± 0.67
T236C		2.73 ± 0.25
B. rise time$_{\Delta F}$ vs. rise time$_{current}$ at indicated pH value		
D347C/T236W 1st	5.5	1.85 ± 0.20
D351C/D237W 1st	**6.5**	**0.79 ± 0.09**
	6.2	**1.10 ± 0.09**
D237C/D347W 1st	**6.3**	**0.82 ± 0.09**
E355C 1st	**6.5**	**0.82 ± 0.14**
	6.3	0.71 ± 0.10
	5.5	**0.77 ± 0.10**
C. rise time$_{\Delta F}$ vs. decay time$_{current}$ at pH6		
K343C/N120W		0.60 ± 0.09
K343C/T236W		**1.13 ± 0.09**
D347C/T236W 1st		0.23 ± 0.02
D347C/T236W 2nd		0.62 ± 0.05
D347C/E238W		0.67 ± 0.05
D237C/D347W 1st		0.18 ± 0.02
D237C/D347W 2nd		0.61 ± 0.06
D351C/D237W 1st		0.15 ± 0.02
D351C/D237W 2nd		0.19 ± 0.02
D351C/F257W		**0.81 ± 0.07**
D237C/D351W		0.40 ± 0.04
E355C 1st		0.06 ± 0.00
E355C 2nd		0.41 ± 0.02
T236C		0.32 ± 0.03

(A-B) For each mutant and pH condition, ΔF rise time values were plotted for individual experiments as a function of the current rise time. *(C)* For each mutant and pH condition, ΔF rise time values were plotted for individual experiments as a function of the current decay time.
The „steepness factor“ for the mutants in this table corresponds to the steepness of linear regressions to these data points; the indicated error is the error of the linear regression; n as indicated in the legends of Figs. 3 and S3B. ΔF and current kinetics were considered as correlated for a given mutant and pH condition if the steepness of the linear regression was not more than a factor of 0.75 different from 1, thus between 0.75 and 1.33 (highlighted in bold).

Table S3. Test for possible intrinsic pH dependence of fluorophores

Mutant	Ratio (%) $\Delta F/F_{desensitized\text{-}to\text{-}open}$ / $\Delta F/F_{closed\text{-}to\text{-}open}$ protocol
T236C	-0.8 ± 3.1
E355C	9.8 ± 2.8
K343C/ N120W^{C}	28.4 ± 1.9
K343C/ T236W	26.9 ± 7.5
D347C/ T236W	17.86 ± 1.9
D347C/ E238W	16.9 ± 4.6
D351C/ D237W^{C}	-11.9 ± 10.0
D351C/ F257W^{C}	31.5 ± 9.4
D237C/D347W^{C*}	26.0 ± 5.0
D237C/D351W^{C}	0.2 ± 3.9

In order to test for a possible intrinsic pH dependence of the fluorophore in the experiment, labeled channels were desensitized by exposing them during 30 s to pH 6.8, before switching to the stimulation pH 6. In this protocol, pH 6 did not induce currents. If a ΔF signal is measured in this protocol, it reflects either an electrically silent transition, or it is due to the intrinsic pH dependence of the fluorophore at its location in the protein. Shown here is the ratio of the ΔF/F of the desensitized-to-open protocol (i.e. pH 6.8 to pH 6) / the ΔF/F of the closed-to-open protocol (i.e. pH 7.4 to pH 6) as percentage, n=3-8. A low ratio indicates that there is no intrinsic pH dependence of the fluorophore, a higher ratio indicates the presence of either electrically silent transitions or of an intrinsic pH dependence of the fluorophore in the experimental conditions. This ratio was measured with the fluorophore AlexaFluor 488 or, where indicated with "^{C}", with CF488A. *, for the mutant D237C/D347W, the indicated values are from 2 experiments at pH 6. At pH 6.2, the ratio was 17.3 ± 9.2 (n=4). The ratio was not measured for the combined VCF/PaC or APc mutants, since they still showed currents after exposure to conditioning pH ≤ 6.8.

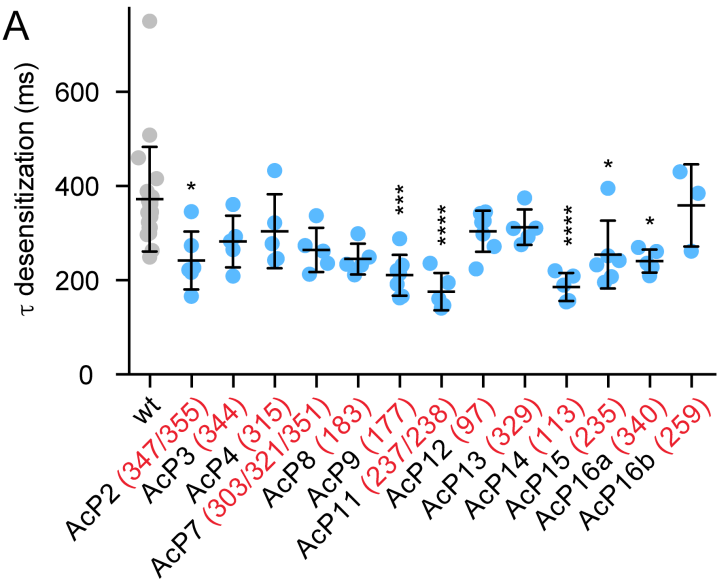
A
τ desensitization (ms)
0
200
400
600
wt
AcP2 (347/355)
AcP3 (344)
AcP4 (315)
AcP7 (303/321/351)
AcP8 (183)
AcP9 (177)
AcP11 (237/238)
AcP12 (97)
AcP13 (329)
AcP14 (113)
AcP15 (235)
AcP16a (340)
AcP16b (259)

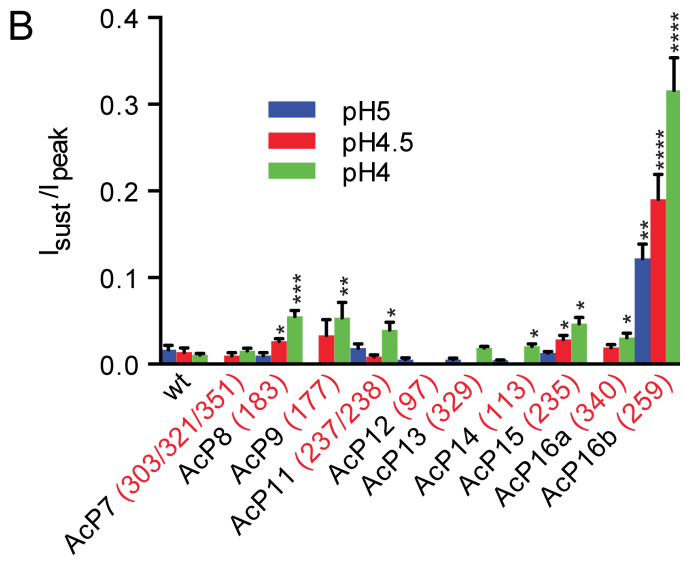
B
I_sust / I_peak
0.0
0.1
0.2
0.3
0.4
pH5
pH4.5
pH4
wt
AcP7 (303/321/351)
AcP8 (183)
AcP9 (177)
AcP11 (237/238)
AcP12 (97)
AcP13 (329)
AcP14 (113)
AcP15 (235)
AcP16a (340)
AcP16b (259)

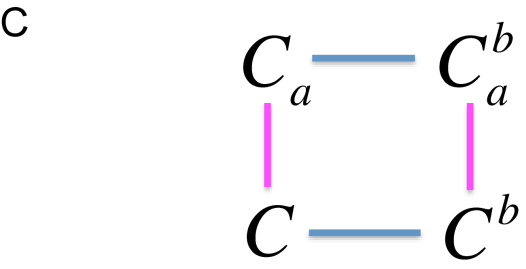
C
C_a
C_a^b
C
C^b

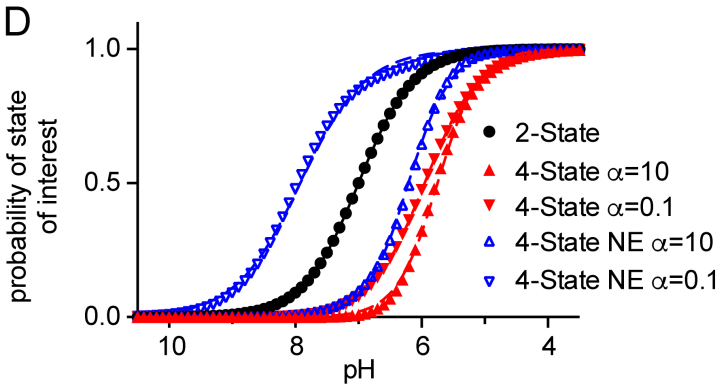
D
probability of state of interest
0.0
0.5
1.0
10
8
6
4
pH
2-State
4-State α=10
4-State α=0.1
4-State NE α=10
4-State NE α=0.1

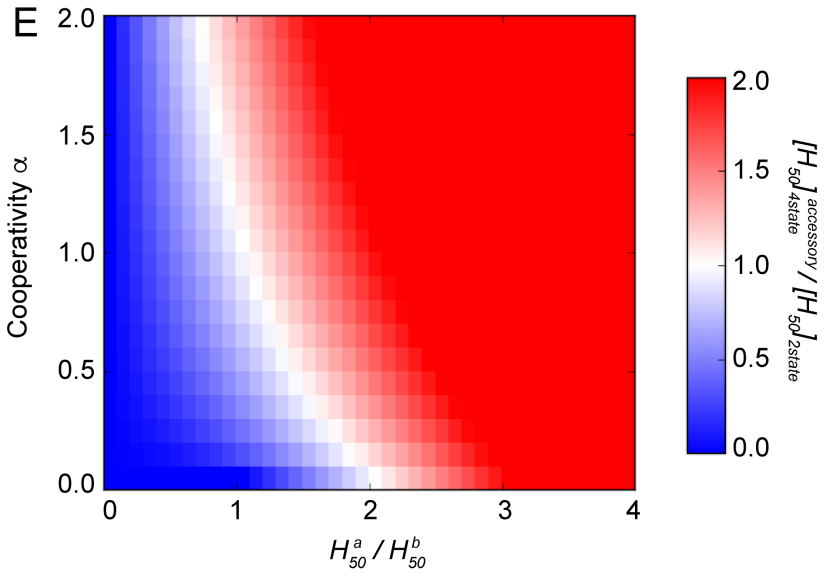
E
Cooperativity α
0.0
0.5
1.0
1.5
2.0
0
1
2
3
4
H_{50}^a / H_{50}^b
$[H]_{50}^{accessory} / [H]_{50}^{2state}$
$[H]_{50}^{4state}$

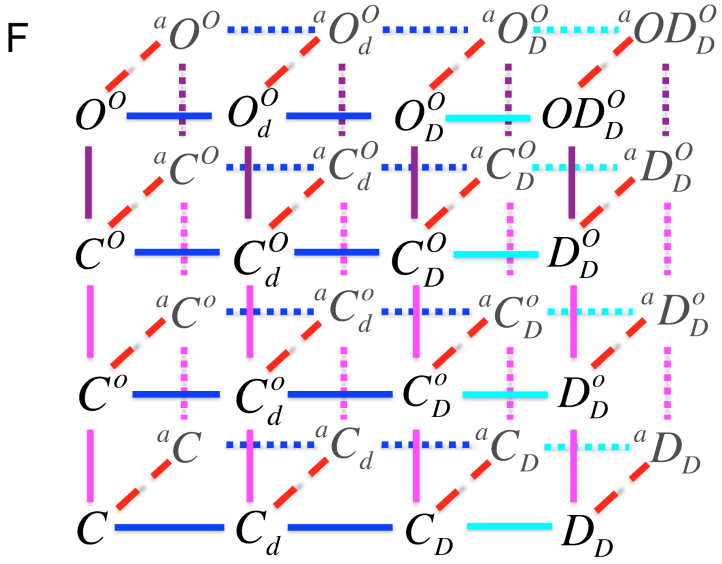
F
$^aO^O$
$^aO_d^O$
$^aO_D^O$
$^aOD_D^O$
O^O
O_d^O
O_D^O
OD_D^O
$^aC^O$
$^aC_d^O$
$^aC_D^O$
$^aD_D^O$
C^O
C_d^O
C_D^O
D_D^O
$^aC^o$
$^aC_d^o$
$^aC_D^o$
$^aD_D^o$
C^o
C_d^o
C_D^o
D_D^o
^aC
^aC_d
^aC_D
^aD_D
C
C_d
C_D
D_D

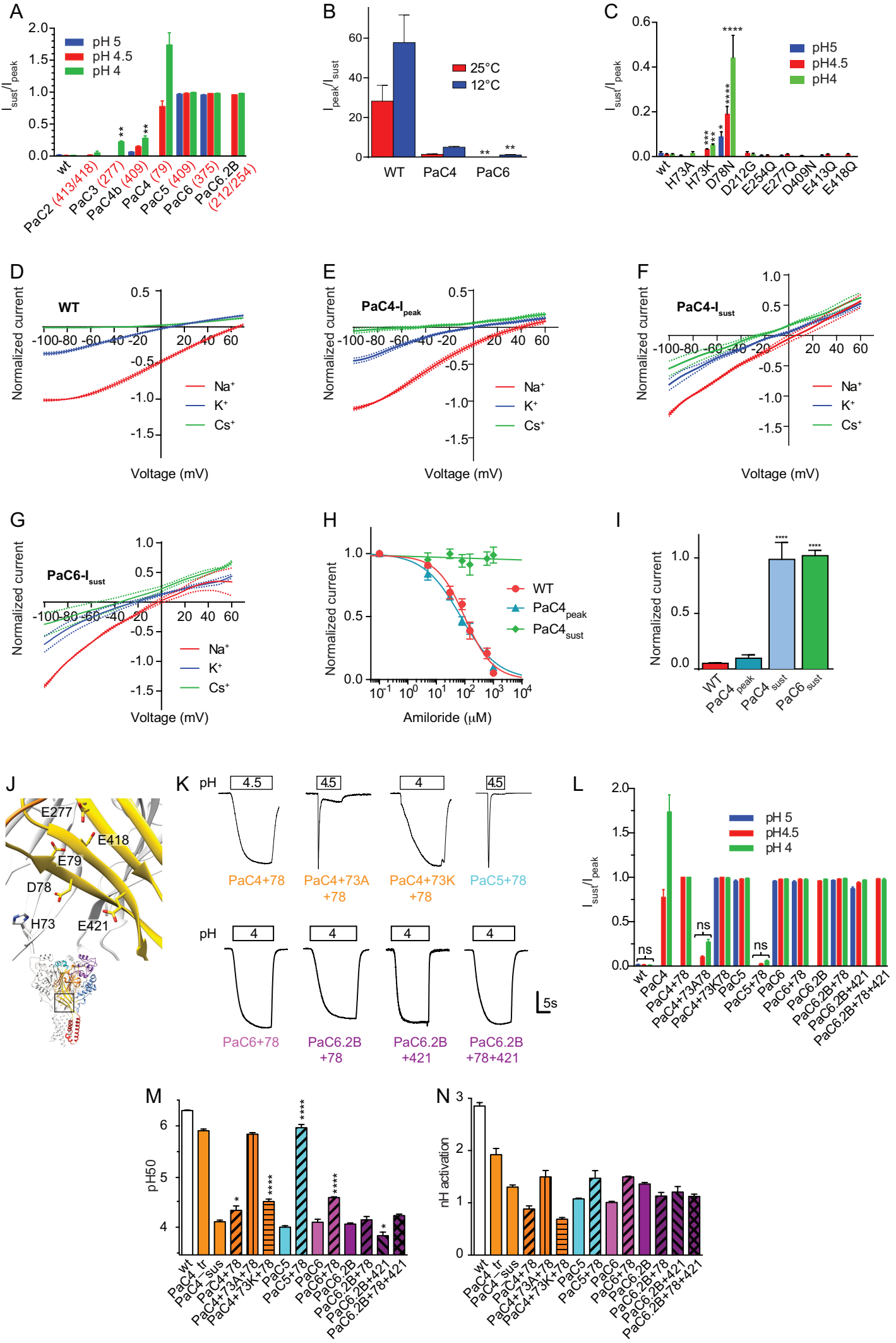
A
pH 5
pH 4.5
pH 4
wt
PaC2 (413/418)
PaC3 (277)
PaC4b (409)
PaC4 (79)
PaC5 (409)
PaC6 (375)
PaC6.2B (212/254)
B
25°C
12°C
WT
PaC4
PaC6
C
pH5
pH4.5
pH4
wt
H73A
H73K
D78N
D212G
E254Q
E277Q
D409N
E413Q
E418Q
D
WT
Na+
K+
Cs+
Normalized current
Voltage (mV)
E
PaC4-Ipeak
F
PaC4-Isust
G
PaC6-Isust
H
WT
PaC4peak
PaC4sust
Amiloride (μM)
I
WT
PaC4 peak
PaC4 sust
PaC6 sust
J
E277
E418
E79
D78
H73
E421
K
pH
PaC4+78
PaC4+73A +78
PaC4+73K +78
PaC5+78
PaC6+78
PaC6.2B +78
PaC6.2B +421
PaC6.2B +78+421
5s
L
pH 5
pH4.5
pH 4
ns
PaC4
PaC4+73A78
PaC4+73K78
PaC5
PaC5+78
PaC6
PaC6+78
PaC6.2B
PaC6.2B+78
PaC6.2B+421
PaC6.2B+78+421
M
pH50
wt
tr
PaC4_sus
N
nH activation

A

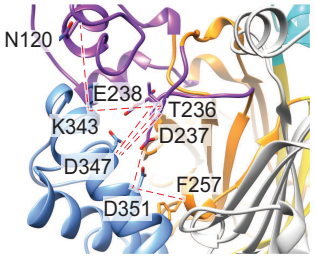

Distances between Cα atoms (Å)

	Open	Desensitized
K343-N120	11.70	11.89
K343-T236	8.32	8.68
D347-T236	9.17	9.43
D347-E238	9.31	9.73
D237-D347	7.01	7.39
D351-D237	9.15	9.36
D351-F257	13.90	14.75

B

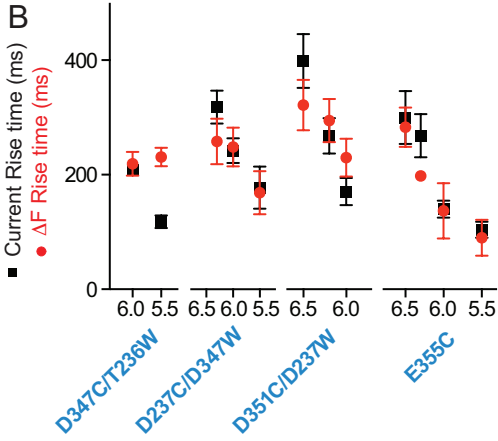

C

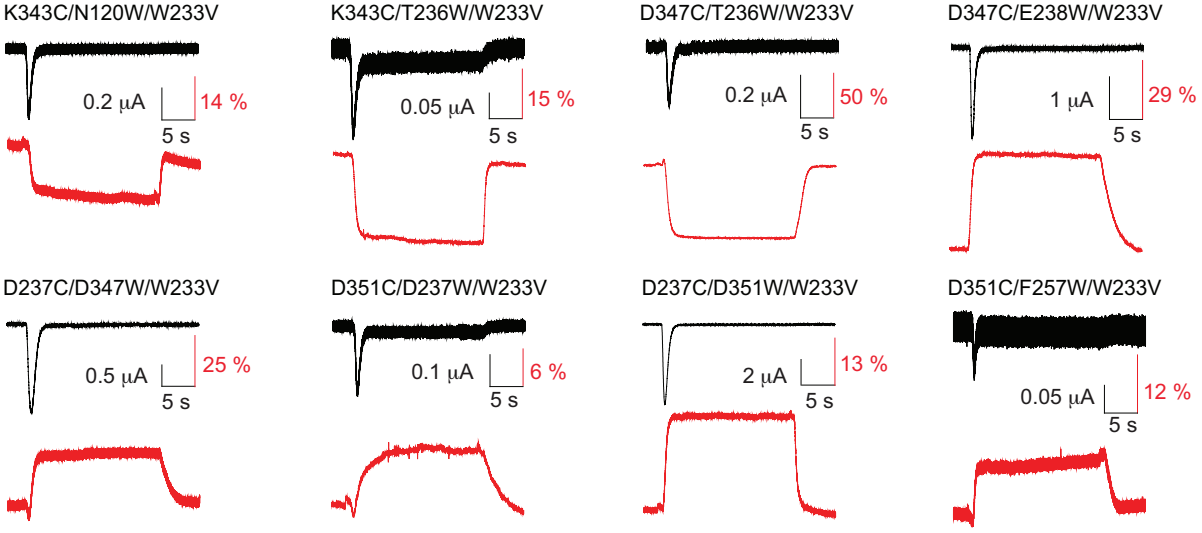

D

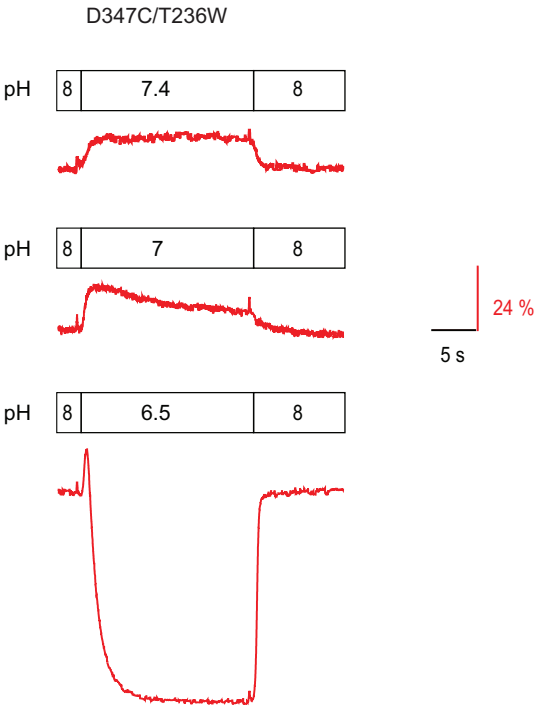

E

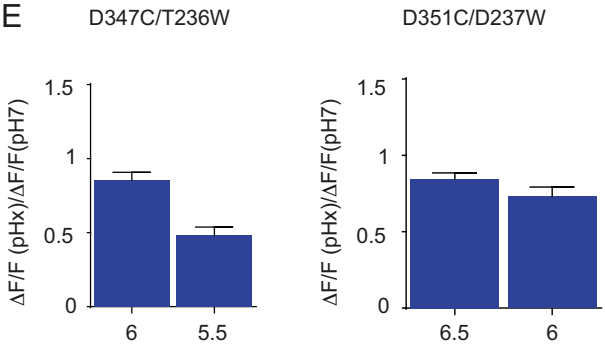

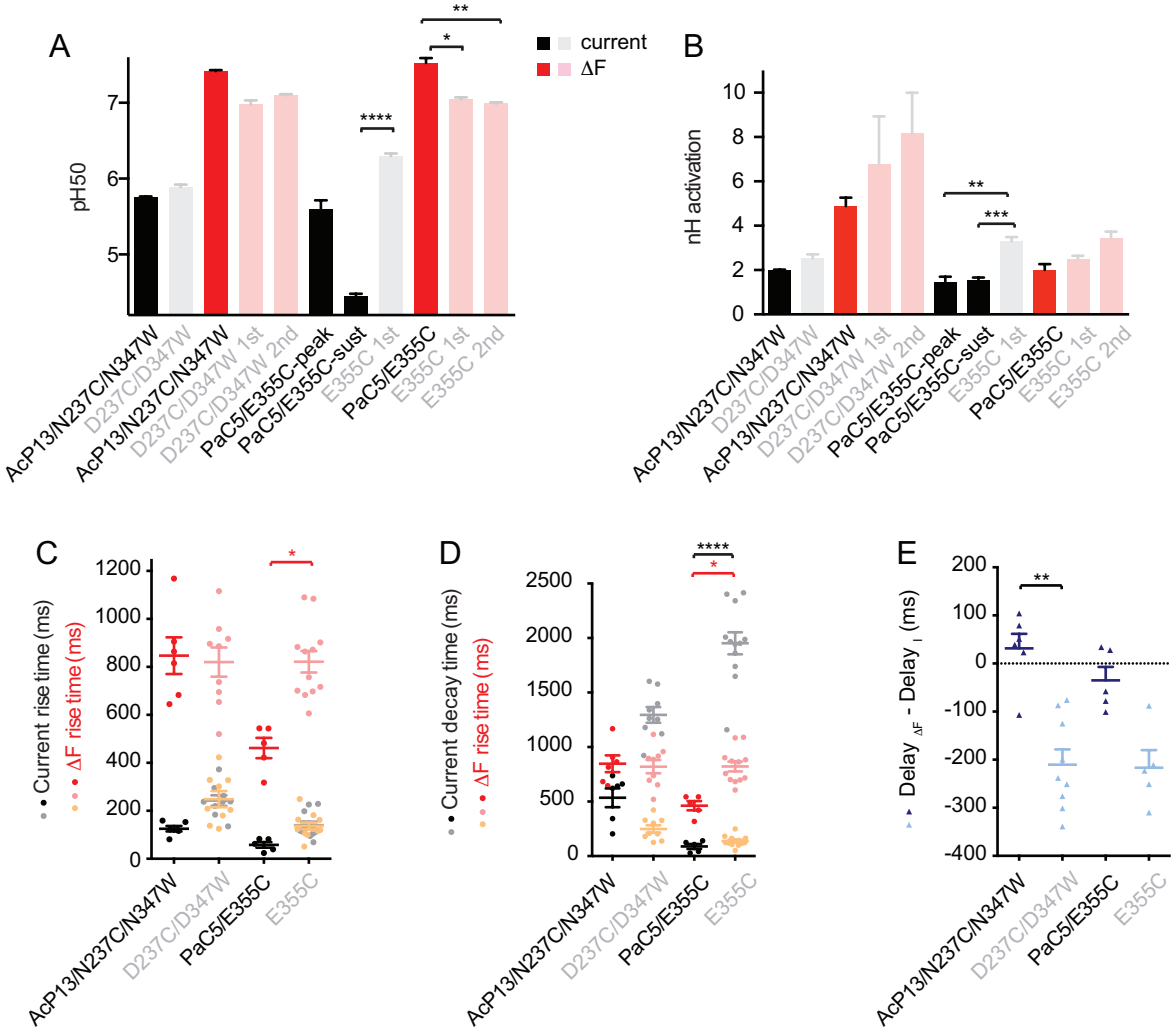
A
pH50
current
ΔF
**
*
****
AcP13/N237C/N347W
D237C/D347W
AcP13/N237C/N347W
D237C/D347W 1st
D237C/D347W 2nd
PaC5/E355C-peak
PaC5/E355C-sust
E355C 1st
PaC5/E355C
E355C 1st
E355C 2nd
B
nH activation
**
***
AcP13/N237C/N347W
D237C/D347W
AcP13/N237C/N347W
D237C/D347W 1st
D237C/D347W 2nd
PaC5/E355C-peak
PaC5/E355C-sust
E355C 1st
PaC5/E355C
E355C 1st
E355C 2nd
C
Current rise time (ms)
ΔF rise time (ms)
*
AcP13/N237C/N347W
D237C/D347W
PaC5/E355C
E355C
D
Current decay time (ms)
ΔF rise time (ms)
****
*
AcP13/N237C/N347W
D237C/D347W
PaC5/E355C
E355C
E
Delay ΔF - Delay I (ms)
**
AcP13/N237C/N347W
D237C/D347W
PaC5/E355C
E355C